Advanced Nonlinear Dynamic Modelling of Bi-stable Composite Plates

Zhangming Wu[1,2*], Hao Li[3*], Michael I. Friswell[4*]

[1]Cardiff School of Engineering, Queens Buildings, The Parade, Newport Road, Cardiff CF24 3AA, UK

[2]School of Aerospace Engineering and Applied Mechanics, Tongji University, 1239 Siping Road, Shanghai 200092, P. R. China

[3] Shanghai Institute of Satellite Engineering, P. R. China

[4] College of Engineering, Swansea University Bay Campus, Fabian Way, Crymlyn Burrows, Swansea SA1 8EN, UK

Corresponding Authors: Zhangming Wu (wuz12@cardiff.ac.uk) and

Hao Li (hithaoli@126.com) and Michael I. Friswell (m.i.friswell@swansea.ac.uk)

Abstract

This paper proposes a novel analytical model to study the nonlinear dynamics of cross-ply bi-stable composite plates. Based on Hamilton's principle, in conjunction with the Rayleigh-Ritz method, an advanced analytical model with only 17 unknown terms is developed to predict the entire nonlinear dynamic response of bi-stable composite plates, which are excited by an electrodynamic shaker. The coupling between the bi-stable plate and the shaker is considered in the development of analytical model. This work, for the first time, simulates the full dynamics of bi-stable plates using an analytical model, including the prediction of the nonlinear characteristics of single well vibration and cross well vibration. Numerical results on three vibrational patterns of two standard cross-ply composite plates are obtained to study the nonlinear dynamics of bi-stable plates. The prediction accuracy on the dynamic characteristics of different vibrational patterns of bi-stable plates are verified by both finite element analysis (FEA) and experimental results. Large amplitude cross-well vibrations due to the transitions between different stable states of bi-stable plates are also characterized accurately. Applying this 17-term analytical model for the dynamic analysis of bi-stable plates is straightforward, as the mass and stiffness properties are obtained directly from the geometry and material properties. Only the damping coefficients for different plates need to be determined from experiments. Furthermore, this proposed 17-term analytical model has much higher computational efficiency than FEA.

1. Introduction

Thin unsymmetric composite plates which exhibit multiple stable static configurations have attracted considerable attention for over three decades [1-4]. A bi-stable fiber reinforced composite plate possesses two stable equilibria, and the plate is able to maintain either of the equilibria without external forces. The bi-stability of composite plates enables large deflections from one equilibrium state to another with small energy input. The static characteristics of unsymmetric bi-stable fiber reinforced plates have been well quantified, after a comprehensive research effort over the last

three decades. Bi-stable composite plates have shown extensive potential applications for morphing aircraft [5-10] and energy harvesting devices [11-13].

Morphing structures change shape to continually optimize operating conditions, according to the environment or loads. In the morphing concepts that take advantage of bi-stable plates, the equilibrium states are matched to shape requirements. Several aero-structures applications with bi-stable morphing airfoils have been proposed and have been experimentally and numerically investigated [5-10]. More recently, research works shed the lights on the dynamic excitation that can trigger the bi-stability of composite plates from one equilibrium state to another with small energy input, for example [14-17]. Recently, the dramatic increase of wireless sensors and electronics, has meant that energy harvesting from ambient vibration has become an active research topic [18, 19]. Nonlinear piezoelectric harvesters have been proposed for broadband energy harvesting. Energy harvesters that employ bi-stable plates as the supporting structure have been proposed. The natural characteristics of bi-stable plates, including the nonlinear bending stiffness and the snap-through phenomenon, are used to increase the power generated and increase the effective frequency range of operation. In particular, the snap-through between equilibrium states gives large velocities that increases the output power [19]. For morphing applications, bi-stable plates are inevitably exposed to high levels of dynamic excitation, and early failure may be induced. Moreover, undesired snap-through may be triggered by the dynamic excitation. For energy harvesting applications, complex vibration patterns including single-well oscillations, chaos and limit cycles are observed in experiments [20]. Lots of research interests had been attracted in the last decade on the investigation of nonlinear dynamic characteristics of bi-stable structures, due to the potential applications in energy harvesting [18-21]. However, modeling the complex nonlinear dynamics of bi-stable composite plates is still an open challenge.

The purpose of this article is to derive a reduced-order analytical model to predict the complex nonlinear dynamics of cross-ply bi-stable composite plates. The nonlinear dynamics of bi-stable plates confined to a single stable state has been experimentally studied by Arrieta et al. [22]. A simple model based on the observed results of two points is established, and captures the complex dynamic phenomenon of the tested bi-stable plates. However the model cannot predict the cross-well dynamics. Later, Arrieta et al. [23] extended the simple model in Ref. [22] by including a piece-wise restoring force in the nonlinear modal equations, to account for the cross-well dynamics of bi-stable plates. It is important to understand the transient shape of bi-stable plates during cross-well oscillations, and the simple models in Refs. [22] and [23] cannot provide the overall response of the plate. Diaconu et al. [24] established an analytical dynamic model of a bi-stable plate using Hamilton's principle, and used it to study the dynamics of the snap-through. The oscillation after snap-through is qualitatively predicted by the model, however, it over predicts the snap-through load by 30% compared to FEA and experiments. Based on Hamilton's principle, Vogl and Hyer [25] established the linear mode prediction model of bi-stable plates, by only retaining the linear terms. The developed analysis generally captures the major features of the lowest vibration mode of the plates. Arrieta et al. [26] developed a low order model for the dynamics of cross-ply plates confined to a stable state. The mode shapes of the stable state are obtained by a Galerkin approach projecting the solution of the nonlinear problem onto the mode shapes of the linear problem. However, the parameters corresponding to the nonlinear terms of the model had to be identified from experimental frequency response functions. Taki et al. [27] established an analytical model to analyze the nonlinear dynamic

behavior of bi-stable composite laminates with $[0–90]_T$ and piezoelectric layers using the Rayleigh–Ritz method and Hamilton's principle. In their modelling, a fourth-order polynomial set of shape functions was used to achieve improved accurate results, which are validated with the finite element method.

A desired dynamic model of a bi-stable plate should be able to quantitatively predict the overall response of its complex dynamics, provided the dimensions, material properties, environmental parameters and the excitation are provided. This study establishes a dynamic model for cross-ply bi-stable plates with high computational efficiency and high accuracy, directly from the plate geometry and material properties. A 17 degrees of freedom dynamic model, derived using Hamilton's principle, is used to investigate the dynamics of bi-stable plates excited at plate center in the transverse direction. Different vibration patterns, distinguished by the snap through phenomenon, are predicted and the corresponding characteristics are discussed. The accuracy of the proposed model is validated by FEA and experiment.

2. Model Derivation

Hamilton's principle is employed to establish the dynamic model for cross-ply bi-stable composite plates. The variation of the Lagrangian function, integrated with respect to time, is set to zero. Thus

$$\int_{t_1}^{t_2} \delta\left(T(t) + W_F(t) - \Pi(t)\right) \mathrm{d}t = 0 \tag{1}$$

where $T(t)$ is the kinetic energy, $W_F(t)$ is the work done by the applied force, and $\Pi(t)$ is the total potential energy.

A typical cross-ply bi-stable plate has two stable cylindrical states and one unstable saddle state. The *x*-*y*-*z* Cartesian coordinate system is employed to describe the problem, as illustrated in Fig. 1. The origin of the coordinate system is at the center of the plate. The *x* and *y* axes are parallel or perpendicular to the fiber directions.

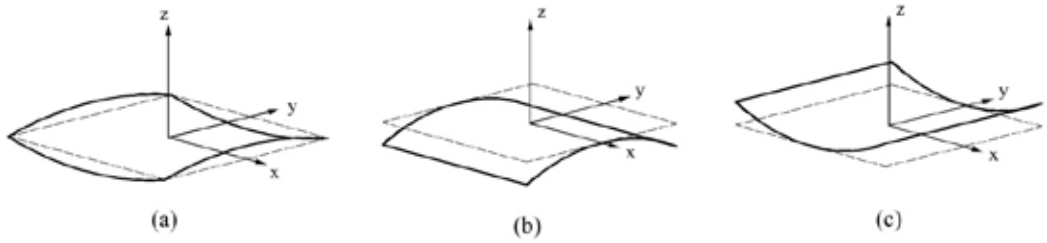

Fig. 1. Sketch of the unstable and stable configurations of a bi-stable cross-ply composite plate and the analysis coordinate system (reproduced from Hyer [3])

The bi-stable plates are assumed to be thin. Thus, the Kirchhoff hypothesis is employed and the layers are assumed to be in the state of plane stress [28]. Hence

$$\begin{Bmatrix} \varepsilon_x \\ \varepsilon_y \\ \gamma_{xy} \end{Bmatrix} = \begin{Bmatrix} \varepsilon_x^0 \\ \varepsilon_y^0 \\ \gamma_{xy}^0 \end{Bmatrix} + z \begin{Bmatrix} k_x \\ k_y \\ k_{xy} \end{Bmatrix} \tag{2}$$

where

$$\mathbf{k} = \begin{Bmatrix} k_x \\ k_y \\ k_{xy} \end{Bmatrix} = \begin{Bmatrix} -\dfrac{\partial^2 w}{\partial x^2} \\ -\dfrac{\partial^2 w}{\partial y^2} \\ -2\dfrac{\partial^2 w}{\partial x \partial y} \end{Bmatrix} \tag{3}$$

represents the plate curvatures. The deflections of bi-stable plates are relative large compared to the plate thicknesses, and hence the geometrical nonlinearity has to be considered in the geometric equation [29]. The mid-plane strains, $\boldsymbol{\varepsilon}^0$, are then defined in the spirit of von Karman, and the in-plane strains of a thin bi-stable plate take the form

$$\boldsymbol{\varepsilon}^0 = \begin{Bmatrix} \varepsilon_x^0 \\ \varepsilon_y^0 \\ \gamma_{xy}^0 \end{Bmatrix} = \begin{Bmatrix} \dfrac{\partial u^0}{\partial x} + \dfrac{1}{2}\left(\dfrac{\partial w}{\partial x}\right)^2 \\ \dfrac{\partial v^0}{\partial y} + \dfrac{1}{2}\left(\dfrac{\partial w}{\partial y}\right)^2 \\ \dfrac{\partial u^0}{\partial y} + \dfrac{\partial v^0}{\partial x} + \dfrac{\partial w}{\partial x}\dfrac{\partial w}{\partial y} \end{Bmatrix} \tag{4}$$

where u^0, v^0 and w denote the in-plane and out-of-plane displacements. The total potential energy of the plate under a thermal-induced load is given by

$$\Pi = \int_{-L_x/2}^{L_x/2} \int_{-L_y/2}^{L_y/2} \left(\frac{1}{2} \begin{bmatrix} \boldsymbol{\varepsilon}^{0\mathrm{T}} & \mathbf{k}^{\mathrm{T}} \end{bmatrix} \begin{bmatrix} \mathbf{A} & \mathbf{B} \\ \mathbf{B} & \mathbf{D} \end{bmatrix} \begin{Bmatrix} \boldsymbol{\varepsilon}^0 \\ \mathbf{k} \end{Bmatrix} - \begin{bmatrix} \mathbf{N}_s^{\mathrm{T}} & \mathbf{M}_s^{\mathrm{T}} \end{bmatrix} \begin{Bmatrix} \boldsymbol{\varepsilon}^0 \\ \mathbf{k} \end{Bmatrix} \right) \mathrm{d}y\mathrm{d}x \tag{5}$$

where L_x and L_y denote plate length and width, respectively, and the explicit time dependence has been omitted. **A**, **B** and **D** are the stretching stiffness matrix, the stretching-bending coupling matrix and the bending stiffness matrix, respectively. $\mathbf{N}_s$ and $\mathbf{M}_s$ are the resultant force and moment due to the thermal stress. The potential energy depends on the in-plane strains $\boldsymbol{\varepsilon}^0$, and the curvatures **k**, which are determined by the assumed displacement functions, u^0, v^0 and w.

The mid-plane strain $\boldsymbol{\varepsilon}^0$, and the bending curvature, **k**, for an unsymmetric plate

are coupled, since the stretching-bending coupling matrix, **B**, is non-zero. If a displacement model for the out-of-plane displacement function, *w*, is assumed, then the mid-plane strains, ε_x^0 and ε_y^0, should have terms which are dependent on *w*, due to the stretching-bending coupling. However, previous studies often applied a generalized modeling approach for unsymmetric plates, where ε_x^0, ε_y^0 and *w* are defined by independent series [30, 31]. However, the influence of stretching-bending coupling on the assumed form of the mid-plane strains, ε_x^0 and ε_y^0, were not explicitly considered. As a result, more terms have to be used in the series expansion of mid-plane strains to achieve better prediction accuracy.

In this study, an alternative procedure is applied to model the mid-plane strains $\boldsymbol{\varepsilon}^0$ for cross-ply bi-stable plates. According to classical lamination theory, the in-plane stress resultants for a thermally-loaded unsymmetric plate is expressed as

$$\mathbf{N} = \mathbf{A}\,\boldsymbol{\varepsilon}^0 + \mathbf{B}\,\mathbf{k} - \mathbf{N}_s^{\mathrm{T}} \tag{6}$$

Equation (6) can be rearranged to give

$$\boldsymbol{\varepsilon}^0 = \mathbf{A}^{-1}\mathbf{N} + \mathbf{A}^{-1}\mathbf{N}_s^{\mathrm{T}} - \mathbf{A}^{-1}\mathbf{B}\,\mathbf{k} = \boldsymbol{\varepsilon}^m + \mathbf{A}^{-1}\mathbf{N}_s^{\mathrm{T}} - \mathbf{A}^{-1}\mathbf{B}\,\mathbf{k} \tag{7}$$

where $\mathbf{A}^{-1}\mathbf{N}$ can be essentially considered as a membrane strain field $\boldsymbol{\varepsilon}^m$. Substituting Eq. (7) into Eq. (5), the total strain energy becomes

$$\begin{aligned}\Pi = \int_{-L_x/2}^{L_x/2}\int_{-L_y/2}^{L_y/2} \Bigg(& \frac{1}{2}\begin{bmatrix}\boldsymbol{\varepsilon}^{m\,\mathrm{T}} & \mathbf{k}^{\mathrm{T}}\end{bmatrix}\begin{bmatrix}\mathbf{A} & \mathbf{0} \\ \mathbf{0} & \mathbf{D}-\mathbf{B}\mathbf{A}^{-1}\mathbf{B}\end{bmatrix}\begin{Bmatrix}\boldsymbol{\varepsilon}^m \\ \mathbf{k}\end{Bmatrix} \\ & -\begin{bmatrix}\mathbf{N}_s^{\mathrm{T}} & \mathbf{M}_s^{\mathrm{T}}\end{bmatrix}\begin{bmatrix}\frac{1}{2}\mathbf{A}^{-1} & -\mathbf{A}^{-1}\mathbf{B} \\ \mathbf{0} & \mathbf{I}\end{bmatrix}\begin{Bmatrix}\mathbf{N}_s \\ \mathbf{k}\end{Bmatrix}\Bigg)\,\mathrm{d}y\mathrm{d}x\end{aligned} \tag{8}$$

This process of reformulating the strain energy into Eq. (8) is analogous to the reduced stiffness matrix (RSB) method [32]. In doing so, the elastic component of total strain energy is decoupled into a stretching part $\frac{1}{2}\boldsymbol{\varepsilon}^{m\,\mathrm{T}}\mathbf{A}\boldsymbol{\varepsilon}^m$ and a bending part $\frac{1}{2}\mathbf{k}\left[\mathbf{D}-\mathbf{B}\mathbf{A}^{-1}\mathbf{B}\right]\mathbf{k}$. Therefore, the deformation of a plate can be decoupled into independent stretching and bending, while the neutral axis does not necessarily lie at the mid-plane, as for a standard isotropic thin shell.

Models that assume constant bending curvatures over predict the plate stiffness [24], and hence non-constant curvatures are assumed in this study. The sixth order out-of-plane displacement $w(t)$ is defined, and the unknown coefficients are again time dependent for the dynamic problem. Thus

$$w(t) = a(t)\,x^2 + b(t)\,y^2 + a_1(t)x^4 + b_1(t)y^4 + a_2(t)x^6 + b_2(t)y^6 + e(t)x^2y^2 \tag{9}$$

where the unknown coefficients, $a_i(t)$, $b_i(t)$ and $e(t)$, represent generalized co-ordinates in the model. The form of $w(t)$ is similar with the form proposed by

Gigliotti *et al.* [33], although the extra term $e(t)x^2y^2$ is included to account for the anticlastic phenomenon near the plate corners.

In this work, instead of taking the mid-plane strains $\boldsymbol{\varepsilon}^0$ as the primary variables in the model, the dynamic stretching strains $\boldsymbol{\varepsilon}^m$ are assumed and expanded up to a sixth order polynomials as

$$\begin{aligned}\varepsilon_x^m(t) &= c(t) + c_1(t)y^2 + c_2(t)y^4 + c_3(t)y^6 + c_4(t)x^2y^2 \\ \varepsilon_y^m(t) &= d(t) + d_1(t)x^2 + d_2(t)x^4 + d_3(t)x^6 + d_4(t)x^2y^2\end{aligned} \tag{10}$$

where the unknown coefficients, $c_i(t)$ and $d_i(t)$, represent generalized co-ordinates in the model. Consequently, the nonlinear dynamic problem of the cross-ply composite plate is modeled by the three variables given in Eqs. (9) and (10), in which there are 17 unknown terms in total.

For $[0_n/90_n]_T$ cross-ply composite plates, $\mathbf{A}^{-1}\mathbf{B}$ and $\mathbf{A}^{-1}\mathbf{N}_s^{\mathrm{T}}$ are explicitly expressed as,

$$-\mathbf{A}^{-1}\mathbf{B} = \mathbf{B}^{-1} = \begin{bmatrix} B^*_{11} & B^*_{12} & 0 \\ B^*_{21} & B^*_{22} & 0 \\ 0 & 0 & 0 \end{bmatrix} = \begin{bmatrix} B^*_{11} & B^*_{12} & 0 \\ -B^*_{12} & -B^*_{11} & 0 \\ 0 & 0 & 0 \end{bmatrix} \tag{11}$$

$$\mathbf{A}^{-1}\mathbf{N}_s^{\mathrm{T}} = \begin{bmatrix} A^{-1}N_{s1}^T \\ A^{-1}N_{s2}^T = A^{-1}N_{s1}^T \\ A^{-1}N_{s3}^T = 0 \end{bmatrix} \tag{12}$$

Substituting Eqs. (11) and (12) into Eq. (7), the mid plane strains are given by

$$\begin{aligned}\varepsilon_x^0 &= \varepsilon_x^m + B^*_{11}k_x + B^*_{12}k_y + A^{-1}N_{s1}^T \\ \varepsilon_y^0 &= \varepsilon_y^m - B^*_{12}k_x - B^*_{11}k_y + A^{-1}N_{s1}^T \\ \gamma_{xy}^0 &= \gamma_{xy}^m\end{aligned} \tag{13}$$

The mid plane displacement functions, $u^0(t)$ and $v^0(t)$, are then derived by integrating with x and y, as

$$\begin{aligned}u^0(t) &= \int\left(\varepsilon_x^0(t) - \frac{1}{2}\left(\frac{\partial w(t)}{\partial x}\right)^2\right)\mathrm{d}x \\ v^0(t) &= \int\left(\varepsilon_y^0(t) - \frac{1}{2}\left(\frac{\partial w(t)}{\partial y}\right)^2\right)\mathrm{d}y\end{aligned} \tag{14}$$

The shear component of mid plane and stretching strains $\gamma_{xy}^{m}(t)$, $\gamma_{xy}^{0}(t)$, are derived by substituting the series forms of $u^{0}(t)$, $v^{0}(t)$ and $w(t)$ into Eq. (2). The polynomial expressions for $u^{0}(t)$, $v^{0}(t)$ and $\gamma_{xy}^{0}(t)$ are given in the Appendix. Note, the constants in $u^{0}(t)$ and $v^{0}(t)$due to integration of strains are treated as 0. Substituting the expressions for $\varepsilon_{x}^{m}(t)$, $\varepsilon_{y}^{m}(t)$ and $\gamma_{xy}^{m}(t)$ into Eq. (8), the dynamic potential energy $\Pi(t)$ is derived. Since the mid plane shear strain $\gamma_{xy}^{0}(t)$ is derived explicitly from the displacement functions, the *compatibility of condition* for the mid-plane strains is satisfied automatically.

The bi-stable composite plates in this study are mounted and excited at the central point. The kinetic energy is defined as

$$T(t)=\frac{1}{2}\rho h\int_{-\frac{Lx}{2}}^{\frac{Lx}{2}}\int_{-\frac{Ly}{2}}^{\frac{Ly}{2}}\left(\frac{d(w_0(t)+w(t))}{dt}\right)^2 dydx \tag{15}$$

where ρ denotes the mass density, $w_0(t)$ denotes the excitation displacement at the central point, and *h* is the thickness of the plate. In Eq. (15), the energy contributions given by the transverse inertia terms are neglected.

In the present study, four constant and equal concentrated transverse forces are applied at the four corners of the plate. In this case, the work done by the applied forces, W_F, is

$$W_F(t)= 4F\left(a(t)\left(\frac{L_x}{2}\right)^2+b(t)\left(\frac{L_y}{2}\right)^2+a_1(t)\left(\frac{L_x}{2}\right)^4+b_1(t)\left(\frac{L_y}{2}\right)^4+a_2(t)\left(\frac{L_x}{2}\right)^6+b_2(t)\left(\frac{L_y}{2}\right)^6+e(t)\left(\frac{L_x}{2}\right)^2\left(\frac{L_y}{2}\right)^2\right) \tag{16}$$

3. Excitation Controlled by Displacement

In the present study, a sinusoidal excitation is applied at the center of the bi-stable plate in the transverse direction. If the bi-stable plate is connected to a structure with great mass and stiffness, the influence from the vibration of the supporting structure can be ignored. In this case, a prescribed excitation displacement $w_0(t)$ is introduced to represent the motion of the supporting structure in the dynamic model. Since there are 17 degrees of freedom in the proposed dynamic model, the generalized displacement is expressed as

$$\mathbf{X}_1(t)=\left[a,b,a_1,b_1,a_2,b_2,e,c,d,c_1,d_1,c_2,d_2,c_3,d_3,c_4,d_4\right]^{\mathrm{T}} \tag{17}$$

According to the Hamilton principle, the variation of the Lagrangian function, given by $\left(T-\Pi-W_F\right)$, is equal to zero. The 17 equations of motion are thus derived, and expressed in the following matrix form

$$\mathbf{M}_1\ddot{\mathbf{X}}_1+\mathbf{D}\left(\dot{\mathbf{X}}_1\right)+\mathbf{K}_1\left(\mathbf{X}_1\right)=\mathbf{F}_1 \tag{18}$$

where $\mathbf{M}_1$ is the mass matrix, $\mathbf{D}\left(\dot{\mathbf{X}}_1\right)$ is the damping force, $\mathbf{K}_1\left(\mathbf{X}_1\right)$ is the nonlinear stiffness force, and the overdot denotes differentiation with respect to time. $\mathbf{F}_1$ denotes the excitation force and also can be expressed by $\mathbf{F}_1=\mathbf{G}\ddot{w}_0$, which is the base excitation force, which depends on the plate inertia and the acceleration $\ddot{w}$. The vector **G** is given in the appendix.

With the definition of the generalized co-ordinates in Eq. (17), and the definition of the displacement models for $u^0\left(t\right)$, $v^0\left(t\right)$ and $w\left(t\right)$ given by Eqs. (9) and (14), the mass matrix $\mathbf{M}_1$ is easily derived. Similarly, the stiffness matrix $\mathbf{K}_1$ is derived by writing the strain energy of the plate, Π, in terms of $\mathbf{X}_1$, and differentiating in the usual way. The expressions of the matrices $\mathbf{M}_1$ and $\mathbf{K}_1$ are given in Appendix. Since the displacement $w\left(t\right)$ is a linear function of the degrees of freedom, the mass matrix $\mathbf{M}_1$ is a constant coefficients matrix.

Damping is very difficult to model precisely, and here the assumption of Rayleigh proportional damping [24] is employed and thus:

$$\mathbf{D}\left(\mathbf{X}_1,\dot{\mathbf{X}}_1\right)=\alpha\,\mathbf{M}_1\dot{\mathbf{X}}_1 \tag{19}$$

where α is the mass proportional damping coefficient. As the vibration of bi-stable plates often occurs at low frequencies, the contribution of stiffness damping is ignored. Thus, only the mass damping effect is considered in this study, and the damping force is a function of velocity alone.

4. Excitation Controlled by Force from a Shaker

In previous studies on the dynamics of bi-stable plates, electrodynamic shakers were often used to excite the plates. Arrieta *et al.* used a transducer between the plate and the shaker to measure the excitation force, and a linear feedback proportional controller was implemented to eliminate the dynamic coupling between the plate and the shaker [23, 34]. As the dynamics of bi-stable plates is nonlinear and complex, it is unlikely that the coupling between the plate and the shaker can be eliminated, completely. In this study, the coupling between the plate and the shaker is explicitly considered using the following analytical model. An electromagnetic shaker consists of a moving part, the armature assembly, a linear spring support for the armature and a dashpot, as illustrated in Fig. 2.

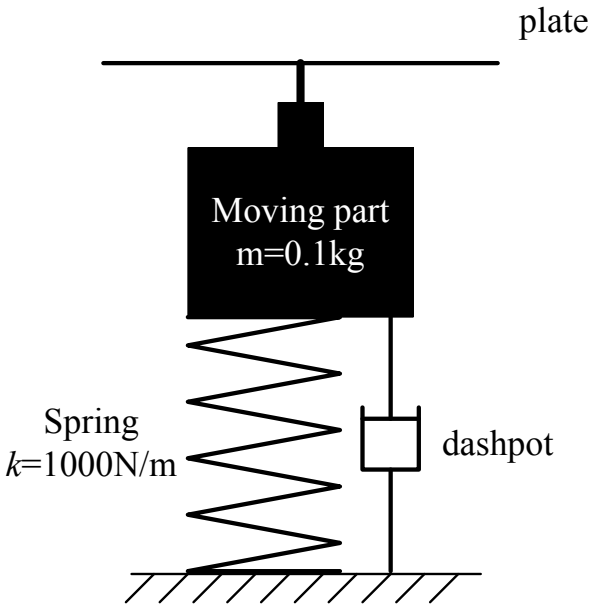

Fig. 2 Dynamic model of the electromagnetic shaker

The single degree of freedom dynamic model of the shaker is given by

$$m\ddot{w}_0 + C\dot{w}_0 + kw_0 = f(t) \tag{20}$$

where m is the mass of the moving armature, C is the damping coefficient of the dashpot, k is the stiffness of the spring system, and $f(t)$ denotes the sinusoidal electromagnetic force of the shaker. Due to the coupling between the shaker and the plate, the oscillation amplitude of the center of the plate, w_0, is unknown. Therefore, the system is a combination of the bi-stable plate and the shaker. There are now 18 degrees of freedom as w_0 is now also included. Thus,

$$\mathbf{X}_2 = \begin{Bmatrix} w_0 \\ \mathbf{X}_1 \end{Bmatrix} \tag{21}$$

The dynamic equations are derived similarly as the process of deriving Eq. (18),

$$\mathbf{M}_2\ddot{\mathbf{X}}_2 + \mathbf{C}\dot{\mathbf{X}}_2 + \mathbf{K}_2(\mathbf{X}_2) = \mathbf{F}_2 \tag{22}$$

Each term in Eq. (22) is expressed in matrix form as

$$\mathbf{C} = \begin{bmatrix} C & \mathbf{0} \\ \mathbf{0} & \alpha\mathbf{M}_1 \end{bmatrix} \tag{23}$$

$$\mathbf{K}_2(\mathbf{X}_2) = \begin{Bmatrix} kX_2(1) \\ \mathbf{K}_1(\mathbf{X}_1) \end{Bmatrix} \tag{24}$$

$$\boldsymbol{F}_2(t) = \begin{bmatrix} f(t) & 0 & \ldots & 0 \end{bmatrix}^{\mathrm{T}} \tag{25}$$

the complete form of $\mathbf{M}_2$ is presented in the Appendix

5. The Effect of Inertial Mass

Inertial masses are often attached to the corners of bi-stable plates to increase the dynamic response. The contribution of these masses (assumed to be equal at each corner) to the kinetic energy is

$$T_{inertia} = \frac{1}{2} m_{inertial} \left[\sum_{i=1}^{4} \dot{w}_i^2 + \sum_{i=1}^{4} \dot{u}_i^2 + \sum_{i=1}^{4} \dot{v}_i^2 \right] \tag{26}$$

where the velocities of each mass (i.e. each corner) are

$$\begin{aligned} \dot{w}_{1,\ldots,4}(t) &= \dot{w}\left(\pm\tfrac{1}{2} L_x, \pm\tfrac{1}{2} L_y, t \right) + \dot{w}_0(t) \\ \dot{u}_{1,\ldots,4}(t) &= \dot{u}^0\left(\pm\tfrac{1}{2} L_x, \pm\tfrac{1}{2} L_y, t \right) \\ \dot{v}_{1,\ldots,4}(t) &= \dot{v}^0\left(\pm\tfrac{1}{2} L_x, \pm\tfrac{1}{2} L_y, t \right) \end{aligned} \tag{27}$$

and $m_{inertial}$ represents the mass added to each corner of the plate. The contribution to the system mass matrix is easily derived. In Eq. (18), the contribution of inertial mass is added to the mass matrix by replacing $\boldsymbol{M}_1$ with $\boldsymbol{M}_1+\boldsymbol{M}_{\text{inertial1}}$. Similarly, the mass matrix $\boldsymbol{M}_2$ should be replaced by $\boldsymbol{M}_2+\boldsymbol{M}_{\text{inertial2}}$ in Eq. (22). The matrices $\boldsymbol{M}_{\text{inertial1}}$ and $\boldsymbol{M}_{\text{inertial2}}$ are given in the Appendix. For the excitation force in Eq. (18), the contribution of the inertial mass $\boldsymbol{F}(\boldsymbol{X}_1)_{inertial}$ is given in the Appendix, and $\boldsymbol{F}(\boldsymbol{X}_1)$ in Eq.(8) is replaced by $\boldsymbol{F}(\boldsymbol{X}_1)+\boldsymbol{F}(\boldsymbol{X}_1)_{inertial}$.

6. Experimental Setup

In the present study, an experiment is established to test the dynamic response of bi-stable composite plates. Figure 3(a) illustrates the schematic diagram of this experimental system, in which each experimental device is connected with respect to the signal (data) flow. Fig. 3(b) shows the practical experimental set up, in which the bi-stable plate is mounted at its centre and excited by a shaker. An accelerometer is attached at the centre of the bi-stable plate to measure the excitation acceleration. A laser vibrometer is used to measure the full dynamic response of the bi-stable plate, and particularly the motion at the plate corners where the 11.54 g inertial masses are attached.

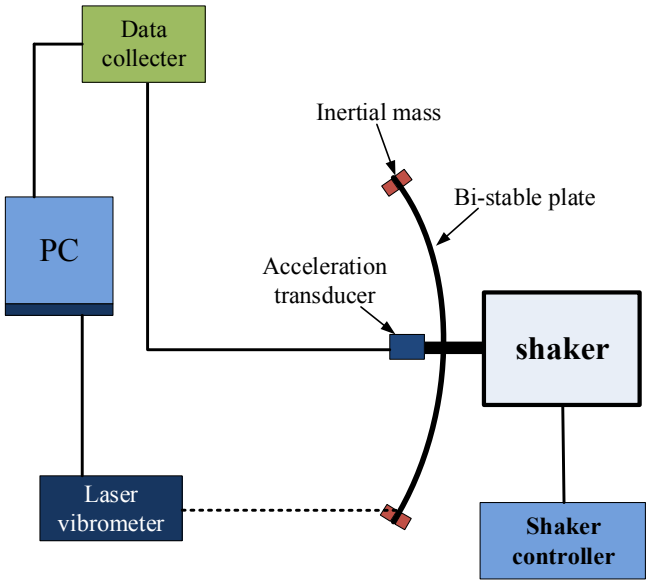

(a) Schematic diagram for the experimental set up

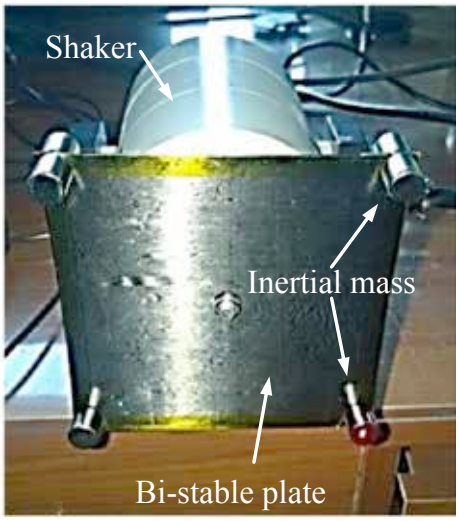

(b) A bi-stable plate with four inertial masses and mounted at the centre.

Fig. 3 The experimental setup

7. Finite Element Analysis

In this study, finite element analysis (FEA) for the bi-stable plates was performed using the commercial tool ABAQUS to validate the proposed analytical model. The S4R shell element (4-node general-purpose shell, reduced integration with hourglass control, finite membrane strains) was chosen to model the bi-stable plates. A mesh density of 40×40 was chosen in the finite element model (FEM) to achieve the required accuracy and efficiency.

A static analysis with two different conditions predicted the stable configurations for the bi-stable plates. In the first "Static" step, a stable configuration is determined under the conditions that the plate cools down from the curing temperature to room

temperature, and a concentrated force along transverse direction is applied at each corner. In the second "Static" step, another stable configuration is obtained for the bi-stable plate, where the transverse concentrated forces are removed, the temperature is kept constant and the second stable configuration is obtained.

After the static analysis, the nonlinear dynamic analysis is performed for the bi-stable plates using the "Dynamic implicit" step in ABAQUS. The plate is mounted at the centre and excited at the centre in the transverse direction. For the case of prescribed excitation displacement, a sinusoidal displacement is applied to the centre of the plate. For the case of excitation by the shaker, a spring and dashpot is connected to the centre of the plate, and a sinusoidal force is applied to the plate centre in the transverse direction, as illustrated in Fig. 4.

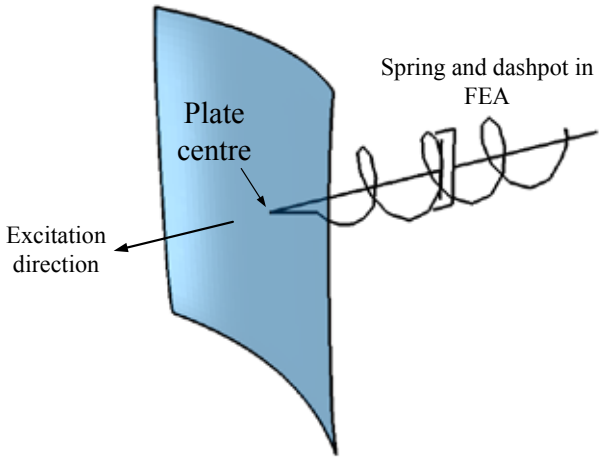

Fig. 4 Schematic of the finite element model of the plate and shaker system

8. Results and Discussion

The bi-stable plates are manufactured using the unidirectional carbon fiber-epoxy matrix prepreg, CCF300/5428. The material properties of the CCF300/5428 prepreg are given in Table 1.

Table 1 Material properties of CCF300/5428 prepreg

CFRP	E_{11}=145 GPa,	E_{22}=9.75 GPa,	G_{12}=5.69 GPa,	ν_{12} =0.312,
	α_{11}= 0.4×10^{-6}/°C,	α_{22} = 25×10^{-6}/°C,	Thickness=0.125mm	

8.1 Static analysis

The static equilibrium shapes of the bi-stable plates need to be determined as the initial states for dynamic analysis. The static equilibrium configurations of the bi-stable plates will be obtained by solving the nonlinear coupled equations

$$\boldsymbol{K}_1(\boldsymbol{X}_1) = \boldsymbol{0} \tag{28}$$

The "FindRoot" function with initial values of $\boldsymbol{X}_1$ is employed in Mathematica® to solve Eq. (28). For the bi-stable plates, there are three groups of solutions, and each group of solutions represents an equilibrium configuration. The actual equilibrium configuration depends on the initial value of the unknowns $\boldsymbol{X}_1$. The stability of the equilibrium solutions need to be checked by the Jacobian matrix, which is positive definite for stable configurations:

$$J = \frac{\partial\left(\boldsymbol{K}_1(\boldsymbol{X}_1)\right)}{\partial\left(\boldsymbol{X}_1\right)} \tag{29}$$

The static stable configurations of the square composite plates 100mm×100mm, $[0_2/90_2]_T$ and 100mm×100mm, $[0_3/90_3]_T$ are analyzed in this section. Each plate is mounted at its centre, and concentrated forces are applied at each corner of the bi-stable plates. The plates cool down from the curing temperature of 180℃ to the room temperature of 20℃. The stable configurations for the bi-stable plates are predicted by both the analytical model and the FEA. The two stable cylindrical mode shapes of each square bi-stable plate are identical in principle, and the only difference lies in the different orientation of the cylindrical deformation which are perpendicular to each other. Fig. 5 and Fig. 6 present the predicted stable states of the two bi-stable plates $[0_2/90_2]_T$ and $[0_3/90_3]_T$, respectively, and show that the stable configurations predicted by the two methods coincide quite well. The numerical results for the out-of-plane deflection at the corners of the bi-stable plates given by the analytical model and the FEA are compared in Table 2. The small errors between the predicted results from the two methods, as shown in Table 2, further validate the proposed analytical model proposed in this work.

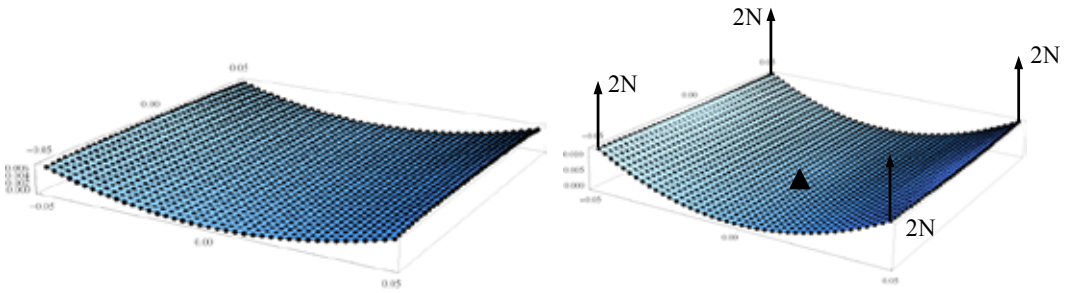

Fig. 5 Predicted stable configurations of the 100mm×100mm, $[0_2/90_2]_T$ plate. FEA results are represented by the black dots, and the theoretical results are represented by the continuous surfaces.

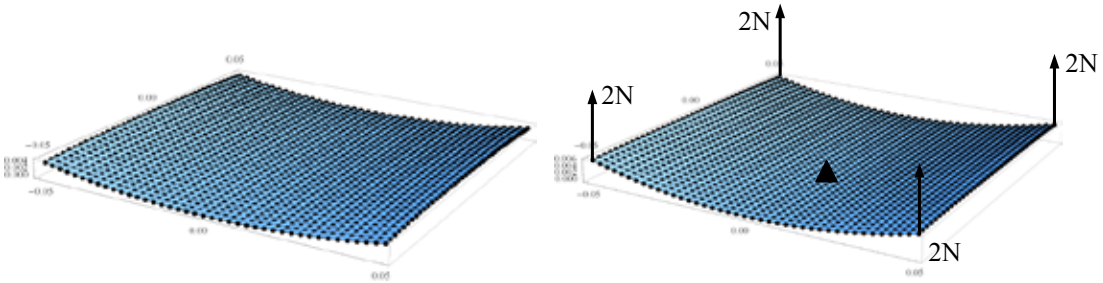

Fig. 6 Predicted stable configurations of the 100mm×100mm, $[0_3/90_3]_T$ plate. FEA results are represented by the black dots, and the theoretical results are represented by the continuous surfaces.

Table 2 Predicted out-of-plane deflection at the corners of the bi-stable plates

Applied Force	**Plate**	**Analytical** (mm)	**FEM** (mm)	**Error** (%)
0N	$[0_2/90_2]_T$	6.68548	6.77379	1.30
	$[0_3/90_3]_T$	3.96181	3.95916	-0.07
0.5N	$[0_2/90_2]_T$	8.12645	8.27471	1.79
	$[0_3/90_3]_T$	4.49868	4.53591	0.82
2N	$[0_2/90_2]_T$	12.3557	12.4621	0.85
	$[0_3/90_3]_T$	5.96985	6.09222	2.01

8.2 Free Vibration

To study the free vibration of the bi-stable plates, four identical concentrated forces are initially applied at each corner of the plates, which are mounted at their centres. The applied forces are the suddenly removed. For the illustration purposes, the numerical results are only determined and presented for the $100\text{mm} \times 100\text{mm}$, $[0_3/90_3]_T$ bi-stable plate. Four inertial masses of 11.54 g are attached to each corner of the bi-stable plates to increase the amplitude of the dynamic response. The static stable configurations of the $[0_3/90_3]_T$ bi-stable plate predicted by the analytical model are shown in Fig. 6, and are used as the initial deformation for the dynamic analysis. The dynamic response of the bi-stable plates requires the solution of Eq. (18). The excitation amplitude at the centre of the plate is zero in the free vibration analysis, i.e. $w_0(t) = 0$. In the FEA, the concentrated forces are applied in the "Static" step, and are removed in the "Dynamic implicit" step. Damping is not considered in either analysis, i.e. $\alpha = 0$.

The free vibration of the $[0_3/90_3]_T$ bi-stable plate subjected to initial concentrated forces of 2N, 0.5N and 0N are predicted. Fig. 7(a) and 7(b) present the oscillation curves at the plate corners determined by the analytical model and the FEA, respectively. Figure 7 shows that the analytical results and the FEA results are very close to each other. When the initial deformation (applied force=0.5N) is small, the plate oscillation is nearly sinusoidal. However, with larger initial deformation (applied force=2N), the oscillation for the bi-stable plate exhibits slightly non-sinusoidal characteristics**.**

The Fast Fourier Transform (FFT) of the predicted vibration presented in Fig. 7 is shown in Fig. 8. For small amplitude excitation (0.5N) there is only one peak, which indicates that the vibration is purely sinusoidal. The first dominant frequency for the analytical model is 44Hz, which is slightly higher than that given by the FEA (42Hz). With larger amplitude excitation (2N), the FFTs have two peaks. The second dominant frequency is twice that of the first dominant frequency, and this indicates the second harmonic vibration. The peak frequencies predicted by the analytical model (40Hz and

80Hz) are slightly higher than those predicted by FEA (38Hz and 76Hz). Moreover, the FFT results in Fig. 8 also illustrate that the first dominant frequency decreases by 4Hz when the oscillation amplitude increases (the applied load increases from 0.5N to 2N). This indicates that the stiffness of the bi-stable plate decreases with respect to increasing oscillation amplitude (i.e. softening), due to the natural nonlinearity of the bi-stable plate. Although the analytical model over predicts the dominant frequencies by about 2Hz, it accurately predicts the nonlinearity of the bi-stable plate. If damping is considered in both the analytical model and the FEM with $\alpha = 100$, the predicted free vibration of the 100mm×100mm, $[0_3/90_3]_T$ plate shown in Fig. 9 is obtained. The decay rates of the vibrations predicted by the two models are nearly identical.

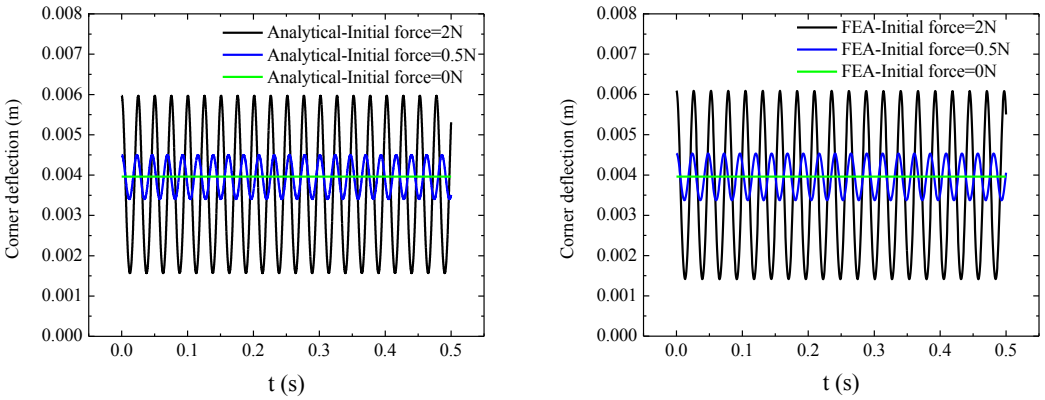

(a) Analytical Analysis (b) FEA

Fig. 7 Predicted free vibration of the 100mm×100mm, $[0_3/90_3]_T$ plate, with zero damping

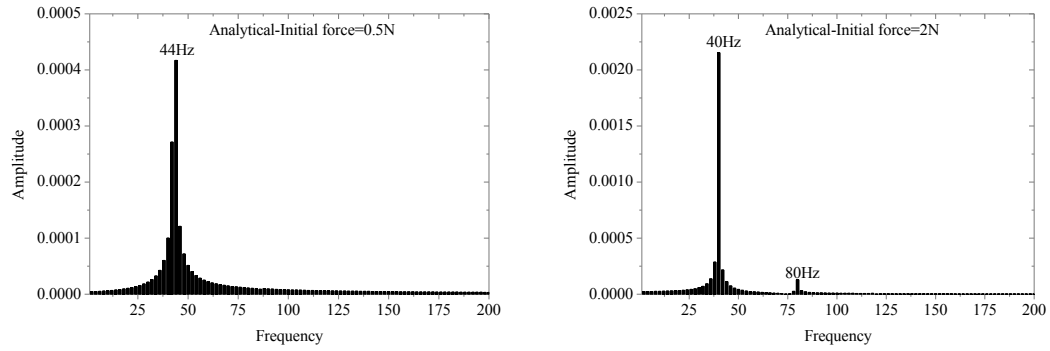

(a) Analytical, initial force=0.5N (b) Analytical, initial force=2N

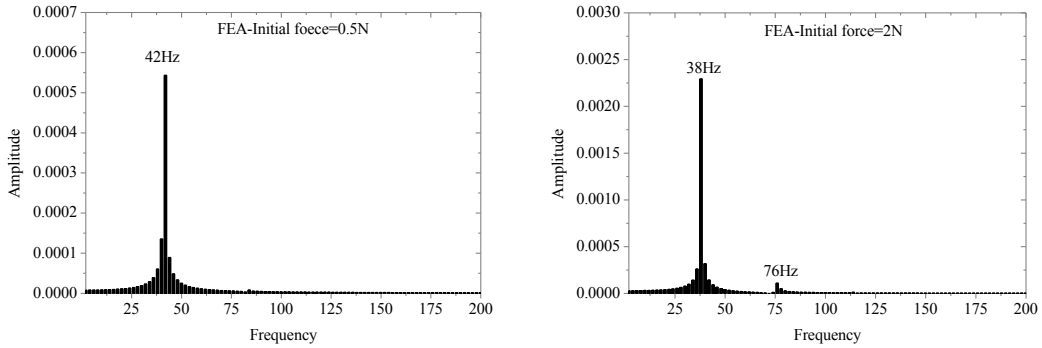

(c) FEA, initial force=0.5N (d) FEA, initial force=2N

Fig. 8 FFT analysis of the predicted free vibration of the $[0_3/90_3]_T$ plate in Fig. 7

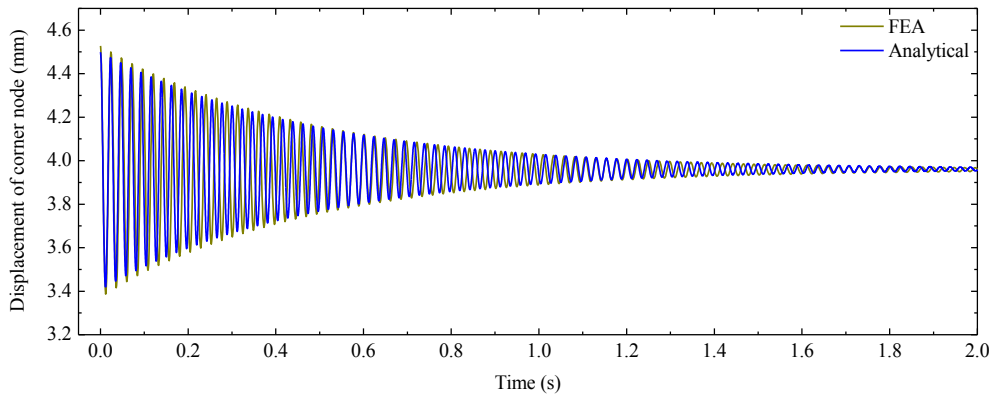

Fig. 9 Predicted free vibration of the 100mm×100mm, $[0_3/90_3]_T$ plate with the proportional damping coefficient $\alpha = 100$

8.3 Single well vibration

The forced vibration of the bi-stable plates within a single energy well is investigated by experiment, analytical model and FEA. The experimental setup for the vibration testing of bi-stable plates is illustrated in Fig. 3. The excitation acceleration

at the plate centre was monitored throughout the experiments. For the low amplitude single well vibration, the excitation acceleration at the plate centre is sinusoidal. The excitation amplitude is adjusted manually from zero to the target level at each frequency. The oscillation amplitudes at the plate corner at different frequencies were recorded by a laser vibrometer, with a fixed level of excitation acceleration for each measurement. The measured vibration amplitudes at the plate corners for the two bi-stable plates ($[0_2/90_2]_T$ and $[0_3/90_3]_T$) are presented in Fig. 10.

Eq. (18) is solved to predict the small amplitude single well vibration of bi-stable plates. Diaconu et al. [24] suggested a measured mass damping coefficient of $\alpha = 83$, although α depends on the plate dimensions, material properties, plate lay-up, etc. Preliminary studies indicate that changing α at these excitation magnitudes has a negligible effect on the stable dynamics of single well vibration if the excitation time is sufficiently long. This benchmark study focuses on the validation of the analytical model against the FEA rather than precisely matching the experimental results. Therefore, a damping coefficient of $\alpha = 100$ is employed. The vibration amplitudes at the plate corners corresponding to different frequencies are predicted using the proposed analytical model and are also shown in Fig. 10.

The single well vibrations at different frequencies are also simulated by FEA. A sinusoidal displacement is applied at the centre of the bi-stable plates in the transverse direction. Compared with the analytical model, the time domain analysis in FEA using the "dynamic implicit" step is very time consuming. The oscillation amplitudes at the plate corners for different excitation frequencies are numerically determined by FEA and are compared with the results predicted by the analytical model, as shown in Fig. 10.

Fig. 10 shows that both the analytical model and the FEA predict only one response peak within the frequency range, whereas extra peaks were observed in the experimental results for each bi-stable plate. To study the origin of the extra resonant peaks in the experimental results, a modal analysis of the bi-stable plates mounted at the centre was performed using FEA. The mode shapes of a square $[0_3/90_3]_T$ bi-stable plate predicted by FEA are presented in Fig. 11. For the first and second modes, the bi-stable plate rotates around its centre. For the third mode, the plate exhibits a symmetric bending deformation, while the plate exhibits an unsymmetric bending deformation along the diagonal line in the fourth mode. Therefore, the common peak in the frequency response function of the bi-stable plate that is predicted by analytical model, FEA and experiment corresponds to the third resonance mode. In FEA, the model is ideal and symmetric, and thus the other modes are not excited in the time domain analysis. Since symmetric displacement function is employed in the analytical analysis, the bi-stable plate is unable to deform in mode 1, mode 2 and mode 4, that are shown in Fig. 11. However, in the experiment the specimen is not ideal and has variabilities in its dimensions and symmetry, including the position of the inertial masses. Therefore, resonance responses occur with respect to the extra vibrational modes, other than mode 3, which were also excited and observed in the experiments. It should be noted that the predicted amplitude-frequency trend of the single well vibration of the bi-stable plate also exhibits nonlinear characteristics, given by a softening stiffness characteristic with increasing vibration amplitude.

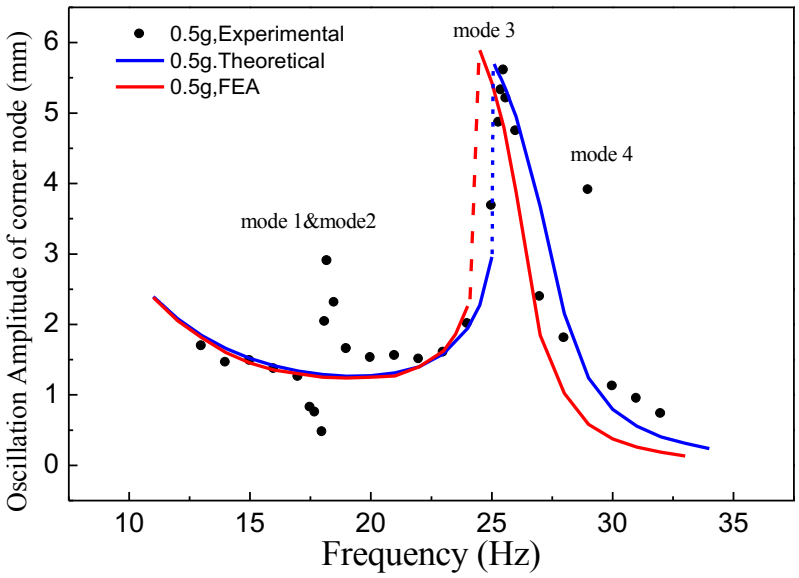

(a) 100mm×100mm, $[0_2/90_2]_T$

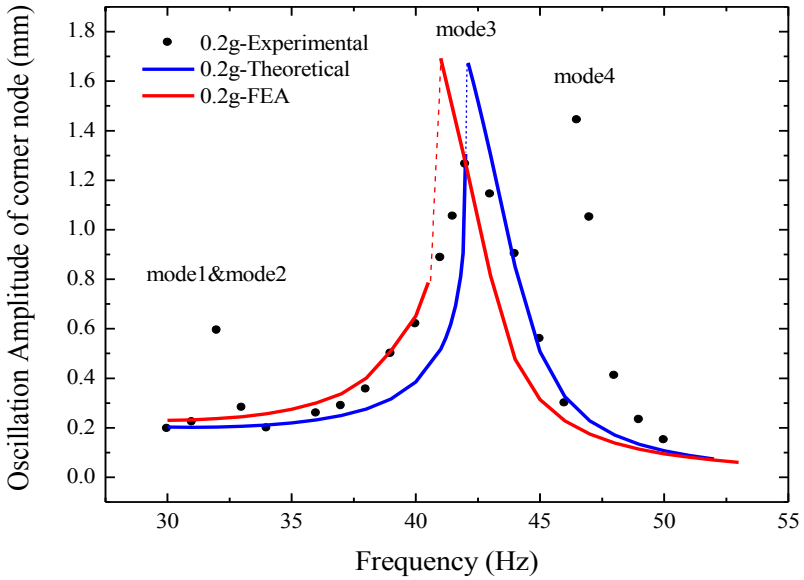

(b) 100mm×100mm, $[0_3/90_3]_T$

Fig. 10 Vibration amplitudes of the bi-stable plates under low level sinusoidal excitation at different frequencies

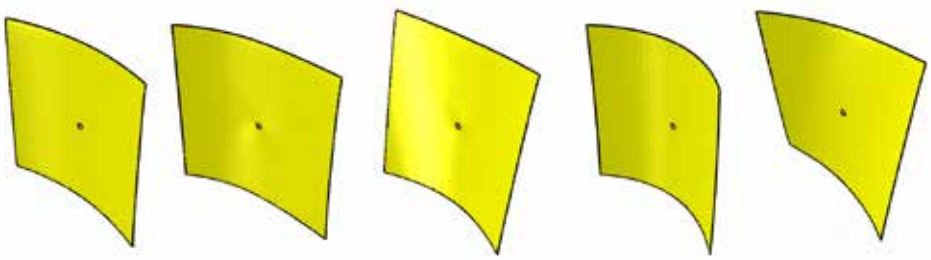

(a) initial shape | (b) mode1 15.29HZ | (c) mode2 15.61Hz | (d) mode 3 41.95Hz | (e) mode 4 46.51Hz

Fig. 11 The first four linear vibration modes about the stable configuration of the square $[0_3/90_3]_T$ bi-stable plate

The predicted and measured displacement of the plate corner for the 100mm×100mm, $[0_2/90_2]_T$ and 100mm×100mm, $[0_3/90_3]_T$ plates are presented in Fig. 12. The dynamic responses predicted by the analytical model agree well with experimental results, and the oscillation curves at the plate corner are almost perfectly sinusoidal.

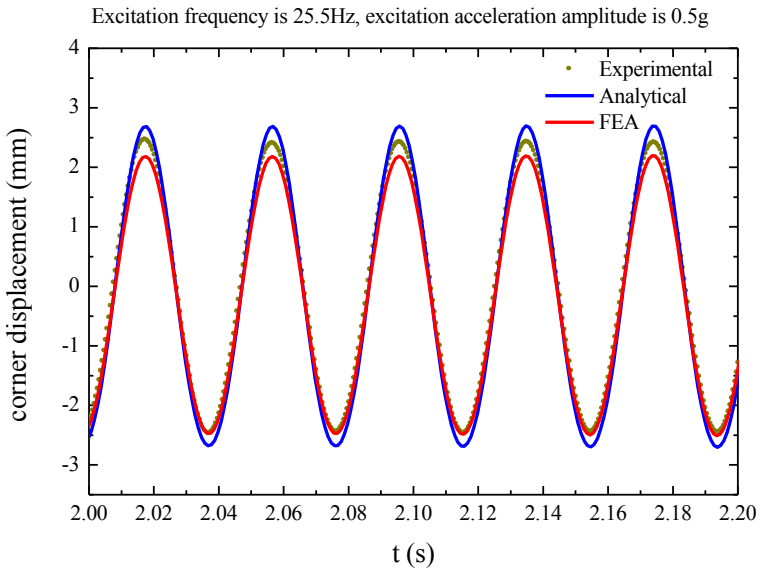

(a) 100mm×100mm, $[0_2/90_2]_T$

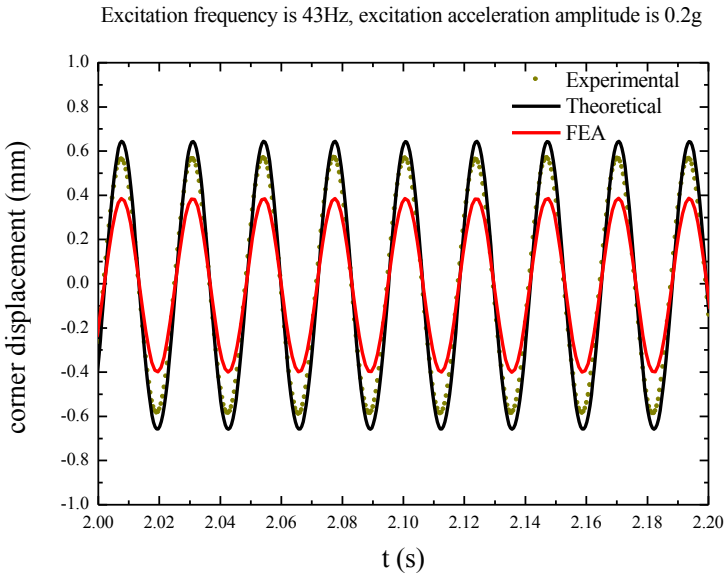

(b) 100mm×100mm, $[0_3/90_3]_T$

Fig. 12 The corner displacement of the bi-stable plates corresponding to single-well oscillation (dT=160℃)

8.4 Cross-well vibration

When the vibration amplitude of the bi-stable plate is larger than a critical level, the dynamic snap-through phenomenon occurs. In other words, the bi-stable plate transforms between the two stable configurations during the vibration. In the present study, if the snap-through phenomenon occurs in each vibration cycle, the vibration pattern is termed continuous cross-well vibration; otherwise, the vibration is termed intermittent cross-well oscillation.

In the experiment, intermittent cross-well oscillation of the 100mm×100mm, $[0_3/90_3]_T$ plate was observed. When the excitation force was increased slowly and achieved a critical value, the vibration pattern of 100mm×100mm, $[0_3/90_3]_T$ plate suddenly transforms from the single-well oscillation to the intermittent cross-well oscillation. This phenomenon is clearly shown in Fig. 13, where the measured excitation acceleration is given as the amplitude increases slowly. During the intermittent cross-well vibration the excitation is no longer sinusoidal and has irregular amplitude. This phenomenon indicates that the bi-stable plate and the shaker are strongly coupled during intermittent cross-well vibration. In this section, Eq. (22) is solved to analytically predict the cross-well vibration of bi-stable plates. In Eq. (22), the excitation displacement $w_0(t)$ is assumed to be unknown and the coupling between the plate and the shaker is considered.

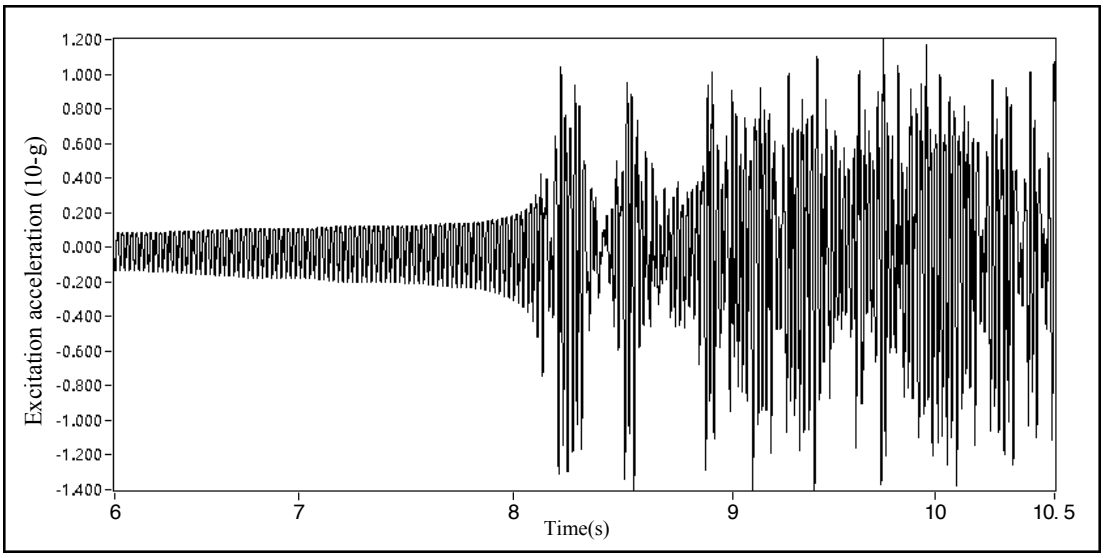

Fig. 13 Experimental acceleration at the centre of the 100mm×100mm, $[0_3/90_3]_T$ plate, at excitation frequency 44 Hz

The nonlinear dynamic response of the 100mm×100mm, $[0_3/90_3]_T$ plate predicted by the analytical model is shown in Fig. 14. The amplitude of the sinusoidal excitation force of the shaker varies linearly with time, that is $F(t) = t \times \sin(44 \times 2\pi t)$. With the increase in the excitation amplitude, the vibration pattern of the bi-stable plate transforms from a single-well oscillation to an intermittent cross-well oscillation, and then to a continuous cross-well oscillation. The analytical model successfully predicts the irregular pattern of the intermittent cross-well vibration at the plate centre, which is also roughly consistent with the nonlinear characteristics observed in the experiment. When the continuous cross-well vibration occurs, the dynamic response of the bi-stable plate becomes regular again.

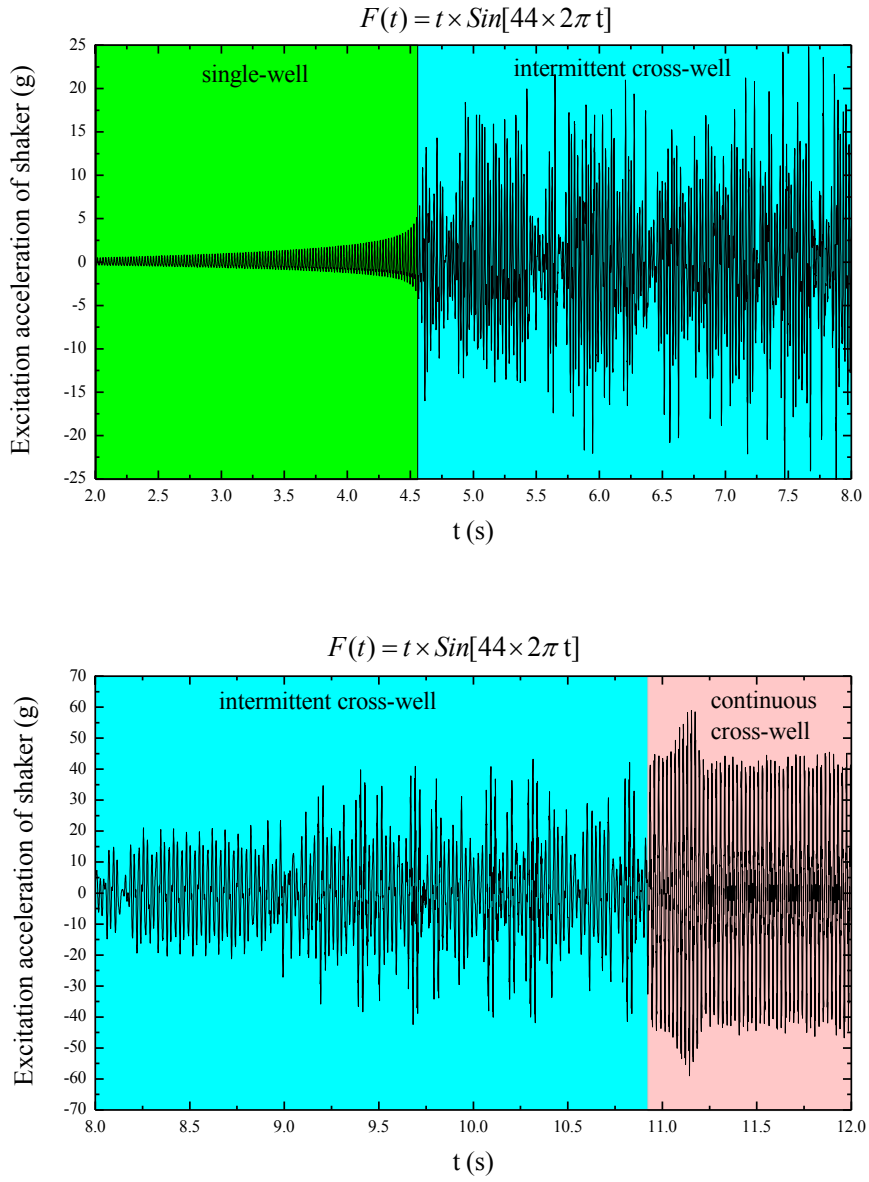

Fig. 14 Acceleration at the centre of the 100mm×100mm, $[0_3/90_3]_T$ plate as the actuation force amplitude linearly increases, at actuation frequency 44 Hz.（dT=160℃, C=5）

The measured and predicted corner displacements of the 100mm × 100mm, $[0_2/90_2]_T$ and 100mm×100mm, $[0_3/90_3]_T$ plates corresponding to intermittent cross-well vibration are compared in Fig. 15. Although the predicted displacements do not match exactly the experimental results, the chaotic characteristics of the intermittent cross-well vibration are very close.

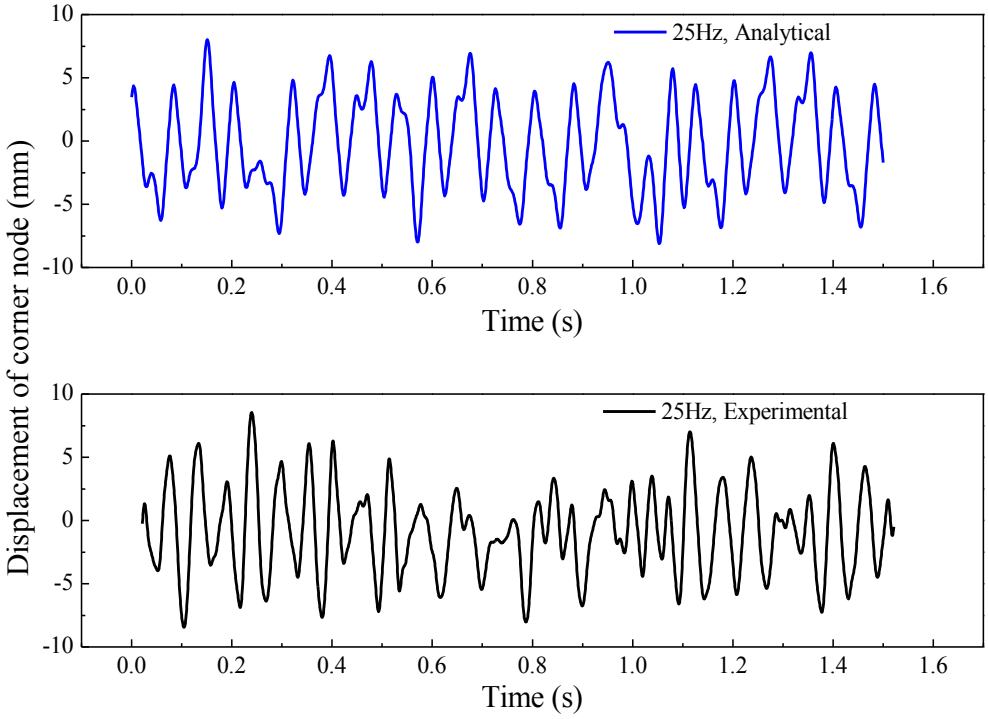

(a) 100mm×100mm, $[0_2/90_2]_T$

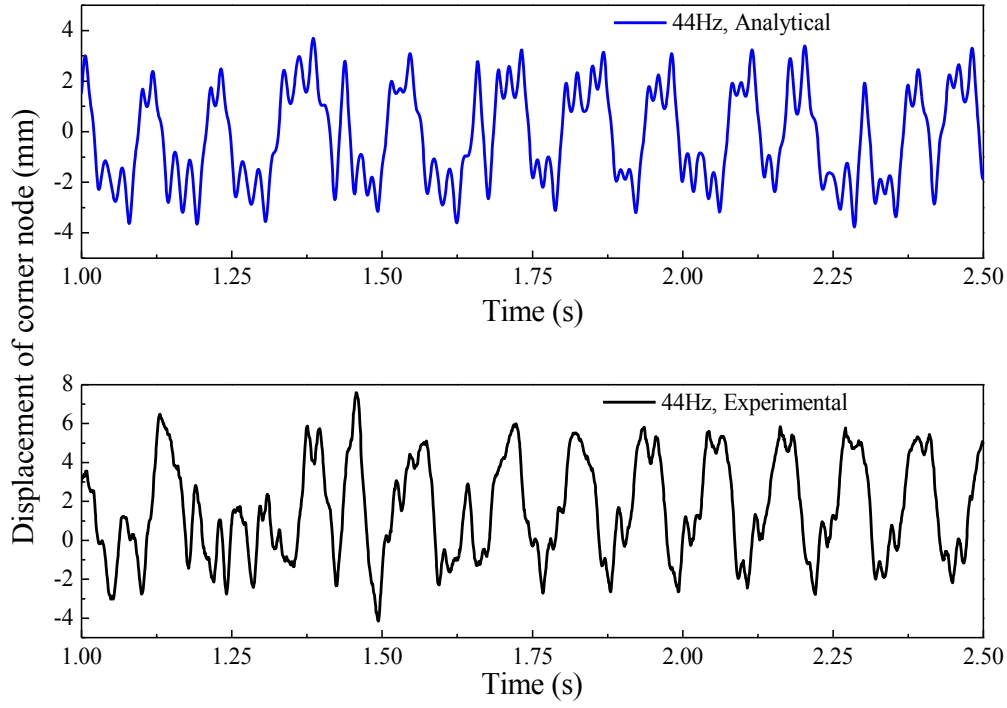

(b) 100mm×100mm, $[0_3/90_3]_T$

Fig. 15 Displacements of the cross-ply bi-stable plates corresponding to intermittent cross-well oscillation

Fig. 16 presents the predicted corner displacements of the 100mm×100mm, $[0_2/90_2]_T$ and 100mm×100mm, $[0_3/90_3]_T$ plates during the continuous cross-well vibration. The excitation force of the shaker is 6N. The continuous cross-well vibrations of these two bi-stable plates also exhibit slight nonlinearity; nevertheless, the cross-well vibration represented by the corner displacements is regular. The FFT analysis for the cross-well vibration of these two bi-stable plates are performed and shown in Fig. 17. The FFT results indicate the presence of the third harmonic. In the experiment, it was difficult to observe the continuous cross-well vibration, as the deflections or dimension asymmetry of the bi-stable plates had an adverse effect on the continuous snap-through event.

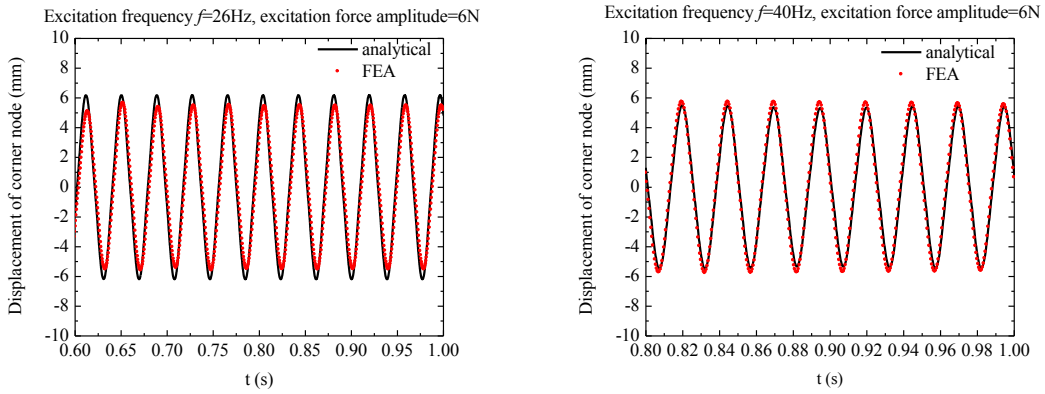

(a) 100mm×100mm, $[0_2/90_2]_T$ (b) 100mm×100mm, $[0_3/90_3]_T$

Fig. 16 Displacement curves of cross-ply bi-stable plate corresponding to cross-well oscillation (dT=160℃, C=5)

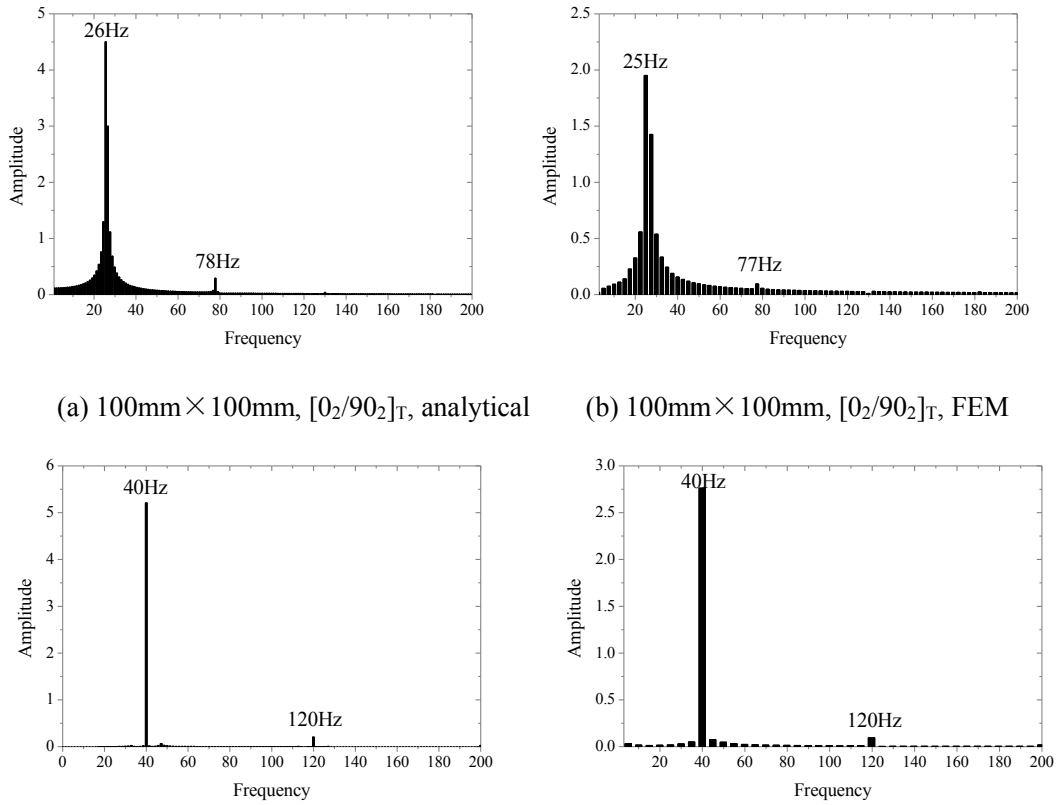

(a) 100mm×100mm, $[0_2/90_2]_T$, analytical (b) 100mm×100mm, $[0_2/90_2]_T$, FEM

(c) 100mm×100mm, $[0_3/90_3]_T$, analytical (d) 100mm×100mm, $[0_3/90_3]_T$, FEM

Fig. 17 FFT of the corner displacements in Fig. 16

The dynamic response of the coupled system of the plate and the shaker does not directly reflect the natural dynamics of the bi-stable plates, whereas the natural dynamics can be obtained by exciting the uncoupled plate with a given displacement input. Specifically, Eq. (18) is applied to study the dynamics of bi-stable plates analytically, since the excitation acceleration of the plate is not coupled with the shaker in the dynamic model represented by Eq. (18). The time domain responses of the $[0_2/90_2]_T$ and $[0_3/90_3]_T$ plates excited by the sinusoidal input $w_0(t)$ are predicted by Eq. (18), and the resulting vibration displacements at the plate corners are plotted in Fig. 18. The excitation amplitude increases by 0.1g in every vibration cycle. The excitation amplitude is linearly varying with time, and the formula for the excitation input is also given in the caption of Fig. 18. The vibration curves in Fig. 18 clearly show that when the excitation amplitude increases to a critical value, the vibration pattern of both plates transfer from the linear sinusoidal vibration to the cross-well vibration. The critical excitation acceleration amplitude, with which the vibration pattern transforms to the cross-well oscillation, for $[0_2/90_2]_T$ plate at 22 Hz is 3.6g, and for $[0_3/90_3]_T$ plate at 35Hz is 3.8g. It is therefore concluded that the analytical model of Eq. (18) is capable to capture the characteristics of the chaotic snap-through and continuous snap through events.

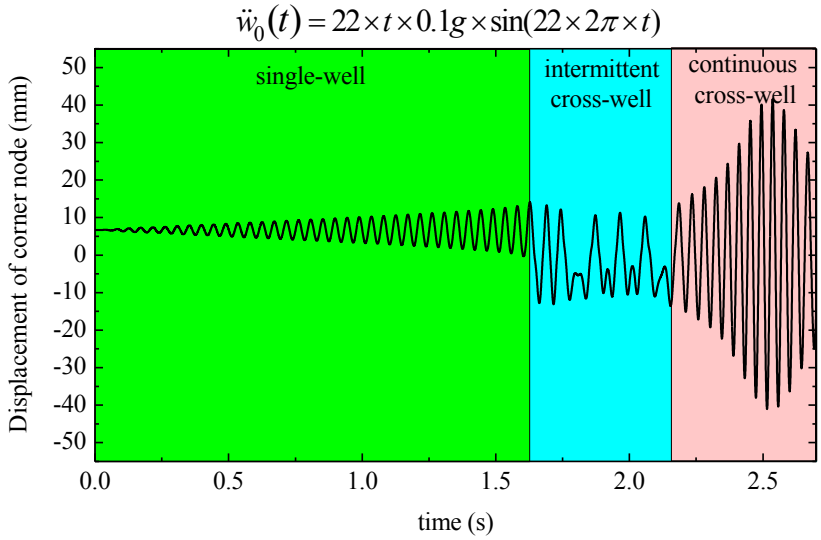

(a) 100mm×100mm, $[0_2/90_2]_T$ plate

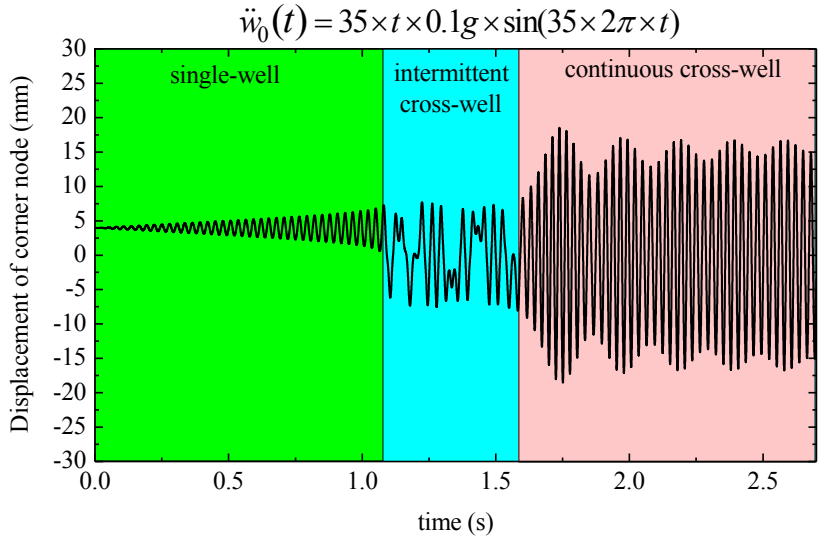

(b) 100mm×100mm, $[0_3/90_3]_T$ plate

Fig. 18 The time domain responses of bi-stable plates excited by a sinusoidal input, predicted by analytical model, i.e. Eq. (18). The excitation amplitude increases by 0.1g in each cycle, excitation acceleration is $\ddot{w}_0(t) = f \times t \times 0.1g \times \sin(f \times 2\pi \times t)$

The dynamic response of 100mm×100mm, $[0_2/90_2]_T$ and $[0_3/90_3]_T$ plates at different frequencies are predicted by both the analytical model given by Eq. (18), and FEA. A constant damping coefficient of $\alpha = 100$ is adopted. Sinusoidal excitations with linearly increased amplitude are applied, that is $\ddot{w}_0(t) = 2t \times 9.8 \times \sin(f \times 2\pi \times \mathrm{t})$. Critical excitation amplitudes to induce cross-well vibration are determined according to the vibration curve of the plate corner, as illustrated in Fig. 18.

The critical excitation amplitudes at different excitation frequencies are predicted by both the analytical model and the FEA, and are compared in Fig. 19. For both plates, the analytical and numerical methods predict identical varying rate of critical excitation

acceleration, and the lowest value. The overall curves given by Eq. (18) are slightly shifted to the right side compared with the FEA curves. The analytical results presented in Fig. 19 indicate that Eq. (18) slightly overestimates the stiffness of the plates. Nevertheless, the results demonstrates that the analytical model is able to accurately predict the nonlinearity of cross-ply bi-stable plates.

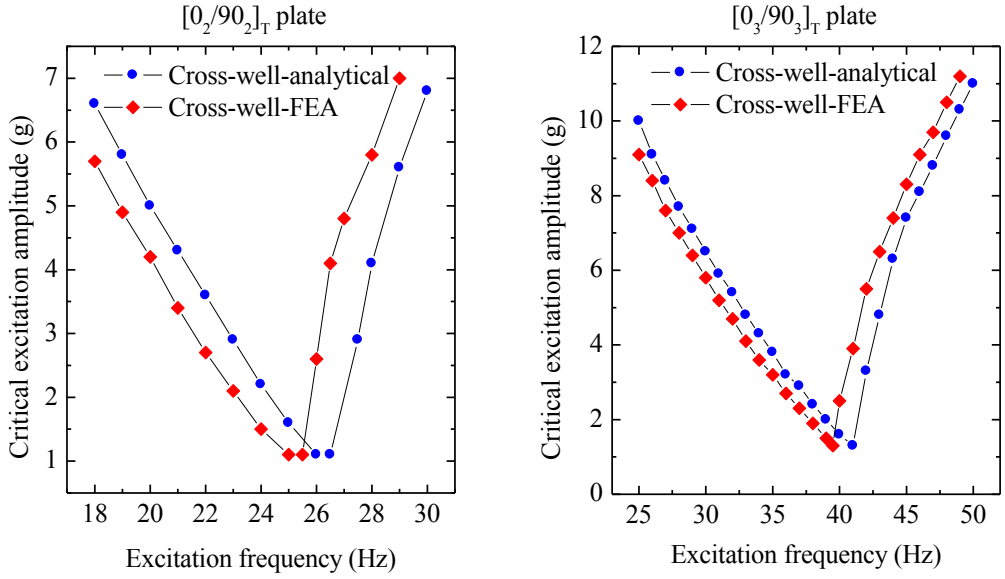

Fig. 19 Critical excitation acceleration needed to induce the cross-well vibrations for the 100mm $\times$100mm, $[0_2/90_2]_T$ and $[0_3/90_3]_T$ plates

8.5 Degree-of-Freedom of the analytical model and its efficiency

In the proposed analytical model, there are 17 terms in the assumed forms of $w(t)$, $\varepsilon_x^m(t)$ and $\varepsilon_y^m(t)$, as presented in Eqs. (9) and (10). The sixth order out-of-plane displacement $w(t)$ is assumed first. In order to test the minimum terms that are required to obtain accurate results, the forms of $\varepsilon_x^m(t)$ and $\varepsilon_y^m(t)$ are initially expanded into complete polynomials. As it is aimed to minimize the unknowns in the analytical model, the terms in $\varepsilon_x^m(t)$ and $\varepsilon_y^m(t)$ are deleted step by step in the testing simulation. After many attempts, it was found that each term left in Eq. (10) is critical and should be remained for obtaining accurate results. It was also interesting to note that, in Eq. (10), $\varepsilon_x^m(t)$ has identical terms of y as $w(t)$, and $\varepsilon_y^m(t)$ has identical terms of x as $w(t)$.

For the illustration purpose, comparison of static load-displacement curves of the 100mm $\times$ 100mm, $[0_3/90_3]_T$ plate predicted using different number of terms in the analytical model. The numerical results are presented in Fig. 20. Concentrated loads are applied on the corners of the plate, which is mounted at the central point. For the 15 degree-of-freedom analytical model, the $c_4(t)x^2y^2$ and $d_4(t)x^2y^2$ terms in $\varepsilon_x^m(t)$ and $\varepsilon_y^m(t)$, i.e. Eq. (10), are deleted. The $c_3(t)y^6$ and $d_3(t)x^6$ terms are

further deleted to reduce the degree-of-freedoms to 13. The 13, 15 and 17 degree-of-freedom in the analytical models have similar precision if the applied loads are smaller or larger than the snap-through load. However, compared to the FEA results, the prediction errors given by the analytical model on the snap through load is increased when the degree-of-freedom is reduced. As the snap through phenomenon occurs in cross-well vibration, inaccurate prediction of snap through will lead to inaccurate dynamic analysis for bistable plates. In contrast, the 17 degree-of-freedom analytical model predicts accurate snap through phenomenon of bistable plates, as it is also validated by the FEA results. This numerical simulation further approves that using 17 terms is the minimum degree-freedom for the analytical model proposed in this work.

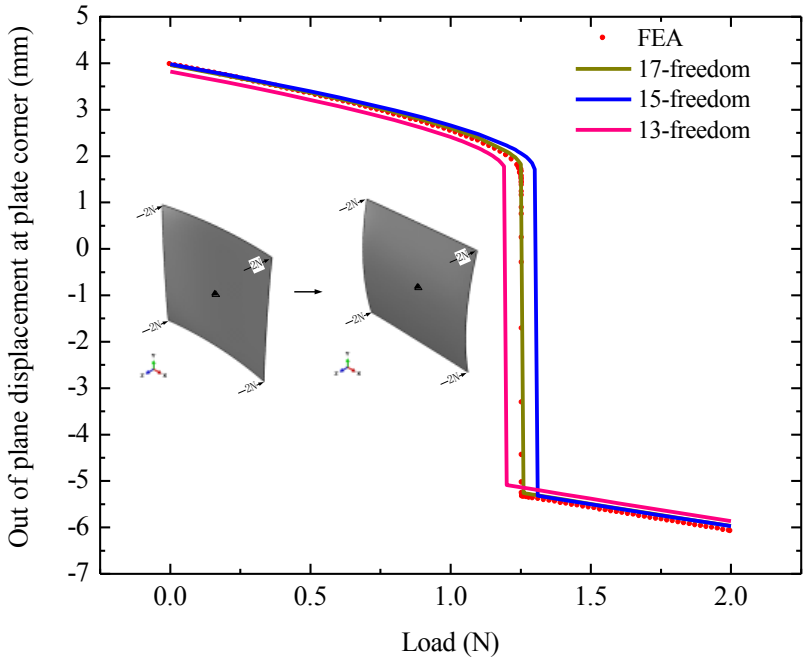

Fig. 20 Static load-displacement curves of the 100mm×100mm, $[0_3/90_3]_T$ plate

In this study, the "NDSolve" function in `Mathematica®` is applied to solve the nonlinear differential equations, i.e. Eqs. (18) and (22). The previous time domain results presented in Figs. 7-18, each of which only requires less than one minute to obtain the results using the proposed analytical model. In contrast, the time-domain dynamic analysis using finite element method is very time-consuming. To obtain more accurate results, the time step in the "Implicit, Dynamic" step should be sufficiently small. In this study, the time step is set to be 0.0025s, therefore a set of numerical results in time domain of 1 second needs 2000 iterations. A cross-well vibration lasting for 2 seconds usually takes 20 to 40 minutes, depending on the mesh size. In Fig. 19, the prediction of critical excitation acceleration by FEA costs much longer computation time than the analytical model. This comparison of computational time demonstrates the high efficiency provided by the analytical model.

9. Conclusion

The dynamics of bi-stable plates are complicated due to the nonlinearity and the snap-through phenomena. Although several dynamic models have been reported, either the dynamic snap-through load was overestimated [24] or the dynamic response

at single points were predicted [22, 23]. An analytical dynamic model with only 17 unknown terms is established based on Rayleigh's method and Hamilton's principle in this study. This established model can accurately predict the nonlinear dynamic response of bi-stable plates. Moreover, this analytical model is able to predict the nonlinear dynamic response over the entire region of bi-stable plates, rather than just few specific points. The influence from the inertial mass and the coupling between a bi-stable plate and the electrical shaker is also considered in the dynamic model. The free vibration, excited vibrations including single-well, intermittent cross-well and continuous cross-well, are predicted and studied. The predicted results of the proposed analytical model for different vibration patterns of bi-stable plates coincide very well with FEA results and experimental results.

The proposed reduced order analytical model for the nonlinear dynamic analysis of composite plates possesses several advantages. Firstly, this proposed analytical model provides a very efficient and effective means to predict the nonlinear dynamics for cross-ply composite bi-stable plates. Secondly, this analytical model is very simple to implement, provided that the material properties and dimensions are provided. Thirdly, the procedure to predict the nonlinear dynamics of bi-stable plates using this analytical model is a relatively simple extension to the static analysis. With only 17 unknown terms, the analytical model is not sophisticated enough to perform very complicated dynamical analysis for bi-stable plates. Nevertheless, an extension of this work to a more general model for angle-ply bi-stable composite plates is straightforward.

Acknowledgement

Zhangming Wu would like to acknowledge the financial support from China's 1000 young scholarship plan. Hao Li sincerely acknowledge the support of National Natural Science Foundation of China Youth Fund, Grant No. 51605299

Appendix

$$
\begin{aligned}
u^0(t) = {} & \left(c(t) + A^{-1}N_{s1}^T\right)x - \frac{2}{3}a(t)^2x^3 - \frac{8}{5}a(t)a_1(t)x^5 - \frac{1}{7}\left(8a_1(t)^2 + 12a(t)a_2(t)\right)x^7 \\
& - \frac{8}{3}a_1(t)a_2(t)x^9 - \frac{18}{11}a_2(t)^2x^{11} + c_1(t)xy^2 + c_2(t)xy^4 + c_3(t)xy^6 \\
& + \frac{1}{3}\left(c_4(t) - 4a(t)e(t)\right)x^3y^2 - \frac{2}{3}e(t)^2x^3y^4 - \frac{8}{5}a_1(t)e(t)x^5y^2 - \frac{12}{7}a_2(t)e(t)x^7y^2 \\
& - 2\left(a(t)B^*_{11} + b(t)B^*_{12}\right)x - \left(4a_1B^*_{11} + \frac{2}{3}e(t)B^*_{12}\right)x^3 - 6a_2(t)B^*_{11}x^5 \\
& - \left(12b_1(t)B^*_{12} + 2e(t)B^*_{11}\right)xy^2 - 30b_2(t)B^*_{12}xy^4
\end{aligned}
\tag{A.01}
$$

$$
\begin{aligned}
v^0(t) &= \left(d(t) + A^{-1}N_{s1}^T\right)y - \frac{2}{3}b(t)^2y^3 - \frac{8}{5}b(t)b_1(t)y^5 - \frac{1}{7}\left(8b_1(t)^2 + 12b(t)b_2(t)\right)y^7 \\
&\quad - \frac{8}{3}b_1(t)b_2(t)y^9 - \frac{18}{11}b_2(t)^2y^{11} + d_1(t)x^2y + d_2(t)x^4y + d_3(t)x^6y \\
&\quad + \frac{1}{3}\left(d_4(t) - 4b(t)e(t)\right)x^2y^3 - \frac{2}{3}e(t)^2x^4y^3 - \frac{8}{5}b_1(t)e(t)x^2y^5 - \frac{12}{7}b_2(t)e(t)x^2y^7 \\
&\quad + 2\left(b(t)B^*_{11} + a(t)B^*_{12}\right)y + \left(4b_1B^*_{11} + \frac{2}{3}e(t)B^*_{12}\right)y^3 - 6b_2(t)B^*_{11}y^5 \\
&\quad + \left(12a_1(t)B^*_{12} + 2e(t)B^*_{11}\right)x^2y + 30a_2(t)B^*_{12}x^4y
\end{aligned} \tag{A.02}
$$

$$
\begin{aligned}
\gamma^0_{xy} &= \left(4a(t)b(t) + 2c_1(t) + 2d_1(t)\right)xy + \left(\frac{2}{3}c_4(t) + 4d_2(t) + 8a_1(t)b(t) + \frac{4}{3}a(t)e(t)\right)x^3y \\
&\quad + \left(\frac{2}{3}d_4(t) + 4c_2(t) + 8a(t)b_1(t) + \frac{4}{3}b(t)e(t)\right)xy^3 + \left(16a_1(t)b_1(t) - \frac{4}{3}e(t)^2\right)x^3y^3 \\
&\quad + \left(6d_3(t) + 12a_2(t)b(t) + \frac{24}{5}a_1(t)e(t)\right)x^5y + \left(6c_3(t) + 12a(t)b_2(t) + \frac{24}{5}b_1(t)e(t)\right)xy^5 \\
&\quad + 24a_2(t)b_1(t)x^5y^3 + 24a_1(t)b_2(t)x^3y^5 + 36a(t)^2b(t)^2x^5y^5 + \frac{60}{7}b_2(t)e(t)xy^7 \\
&\quad + \frac{60}{7}a_2(t)e(t)x^7y + \left(24a_1(t)B^*_{12} - 24b_1(t)A^{-1}B^*_{12}\right)xy + 120a_2(t)B^*_{12}x^3y \\
&\quad - 120b_2(t)B^*_{12}xy^3
\end{aligned} \tag{A.03}
$$

$$
\boldsymbol{M}_1 = \rho h\int_{-\frac{Lx}{2}}^{\frac{Lx}{2}}\int_{-\frac{Ly}{2}}^{\frac{Ly}{2}}\left(\frac{\partial w(t)}{\partial \boldsymbol{X}_1(i)}\frac{\partial w(t)}{\partial \boldsymbol{X}_1(j)}\right)dydx, i, j = 1 \sim 17 \tag{A.04}
$$

$$
\boldsymbol{K}_1(\boldsymbol{X}_1) = \left\{\frac{\partial(\Pi(t)_{plate} - W_F(t))}{\partial X_1(\mathrm{i})}\right\}, i = 1 \sim 17 \tag{A.05}
$$

$$
\boldsymbol{G} = -\rho h\int_{-\frac{Lx}{2}}^{\frac{Lx}{2}}\int_{-\frac{Ly}{2}}^{\frac{Ly}{2}}\left\{\frac{\partial w(t)}{\partial \boldsymbol{X}_1(i)}\right\}dydx, i = 1 \sim 17 \tag{A.06}
$$

$$
\mathbf{M}_2 = \begin{pmatrix} m & \mathbf{0} \\ \mathbf{0} & \mathbf{0} \end{pmatrix} + \rho h\int_{-\frac{Lx}{2}}^{\frac{Lx}{2}}\int_{-\frac{Ly}{2}}^{\frac{Ly}{2}}\begin{pmatrix} 1 & \dfrac{\partial w(t)}{\partial \boldsymbol{X}_2(i)} \\ \dfrac{\partial w(t)}{\partial \boldsymbol{X}_2(j)} & \dfrac{\partial w(t)}{\partial \boldsymbol{X}_2(i)}\dfrac{\partial w(t)}{\partial \boldsymbol{X}_2(j)} \end{pmatrix}dxdy \qquad i, j = 2 \sim 18 \tag{A.07}
$$

$$
\boldsymbol{M}_{inertial1} = 4m_{inertial}\left(\frac{\partial w\left(\frac{Lx}{2}, \frac{Ly}{2}, t\right)}{\partial X_1[i]}\frac{\partial w\left(\frac{Lx}{2}, \frac{Ly}{2}, t\right)}{\partial X_1[j]}\right), i, j = 1 \sim 17 \tag{A.08}
$$

$$\boldsymbol{M}_{inertial2} = 4m_{inertial}\begin{pmatrix} 1 & \dfrac{\partial w\left(\frac{Lx}{2},\frac{Ly}{2},t\right)}{\partial X_2(i)} \\ \dfrac{\partial w\left(\frac{Lx}{2},\frac{Ly}{2},t\right)}{\partial X_2(j)} & \dfrac{\partial w\left(\frac{Lx}{2},\frac{Ly}{2},t\right)}{\partial X_2(i)}\dfrac{\partial w\left(\frac{Lx}{2},\frac{Ly}{2},t\right)}{\partial X_2(j)} \end{pmatrix}, i,j = 2\sim 18 \quad \text{(A.09)}$$

$$\boldsymbol{F}(\boldsymbol{X}_1)_{inertial} = -4m_{inertial}\frac{d^2(w_0(t))}{dt^2}\left\{\frac{\partial w\left(\frac{Lx}{2},\frac{Ly}{2},t\right)}{\partial X(\mathrm{i})}\right\}, i = 1\sim 17 \quad \text{(A.10)}$$

Reference

1. Emam, S.A. and D.J. Inman, *A Review on Bistable Composite Laminates for Morphing and Energy Harvesting.* Applied Mechanics Reviews, 2015. **67**(6): p. 060803.
2. Hyer, M.W., *Some observations on the cured shape of thin unsymmetric laminates.* Journal of Composite Materials, 1981. **15**(2): p. 175-194.
3. Hyer, M.W., *The room-temperature shapes of four-layer unsymmetric cross-ply laminates.* Journal of Composite Materials, 1982. **16**(4): p. 318.
4. Ren, L., A. Parvizi-Majidi, and Z. Li, *Cured Shape of Cross-Ply Composite Thin Shells.* Journal of Composite Materials, 2003. **37**(20): p. 1801-1820.
5. Dano, M.-L., M. Jean-St-Laurent, and A. Fecteau, *Morphing of bistable composite laminates using distributed piezoelectric actuators.* Smart Materials Research, 2012. **2012**.
6. Daynes, S., P. Weaver, and J. Trevarthen, *A morphing composite air inlet with multiple stable shapes.* Journal of Intelligent Material Systems and Structures, 2011: p. 1045389X11399943.
7. Pirrera, A., D. Avitabile, and P. Weaver, *On the thermally induced bistability of composite cylindrical shells for morphing structures.* International journal of solids and structures, 2012. **49**(5): p. 685-700.
8. Kim, S.-W., et al. *Towards a bio-mimetic flytrap robot based on a snap-through mechanism*. in *Biomedical Robotics and Biomechatronics (BioRob), 2010 3rd IEEE RAS and EMBS International Conference on*. 2010. IEEE.
9. Daynes, S., et al., *On a Bistable Flap for an Airfoil*, in *50th AIAA/ASME/ASME/ASCE/AHS/ASC Structure, Structure Dynamics, and Materials Conference*. 2009, American Institute of Aeronautics and Astronautics.
10. G.Diaconu, C., P. M.Weaver, and F. Mattioni, *Concepts for morphing airfoil sections using bi-stable laminated composite structures.* Thin Walled Structures, 2007. **11**: p. 1-13.

11. Arrieta, A.F., et al., *A cantilevered piezoelectric bi-stable composite concept for broadband energy harvesting*, in *SPIE Smart Structures and Materials+ Nondestructive Evaluation and Health Monitoring*. 2013, International Society for Optics and Photonics: San Diego, California p. 86880G-86880G-9.

12. Arrieta, A.F., et al., *Broadband vibration energy harvesting based on cantilevered piezoelectric bi-stable composites.* Applied Physics Letters, 2013. **102**(17): p. 173904.

13. Li, H., F. Dai, and S. Du, *Broadband energy harvesting by exploiting nonlinear oscillations around the second vibration mode of a rectangular piezoelectric bistable laminate.* Smart materials and structures, 2015. **24**(4): p. 045024.

14. Arrieta, A.F., D.J. Wagg, and S.A. Neild, *Dynamic Snap-through for Morphing of Bi-stable Composite Plates.* Journal of Intelligent Material Systems and Structures, 2011. **22**(2): p. 103-112.

15. Onur, B., et al., *Dynamic control of a bistable wing under aerodynamic loading.* Smart Materials and Structures, 2013. **22**(2): p. 025020.

16. Simsek, M.R. and O. Bilgen, *Hybrid Position Feedback Controller for Inducing Cross-Well Motion of Bistable Structures.* AIAA Journal, 2016. **54**(12): p. 4011-4021.

17. Zarepoor, M. and O. Bilgen, *Constrained-Energy Cross-Well Actuation of Bistable Structures.* AIAA Journal, 2016. **54**(9): p. 2905-2908.

18. Arrieta, A., et al., *A piezoelectric bistable plate for nonlinear broadband energy harvesting.* Applied Physics Letters, 2010. **97**(10): p. 104102.

19. Pellegrini, S.P., et al., *Bistable vibration energy harvesters: A review.* Journal of Intelligent Material Systems and Structures, 2012. **24**(11): p. 1303-1312.

20. Betts, D.N., et al., *Nonlinear dynamics of a bistable piezoelectric-composite energy harvester for broadband application.* The European Physical Journal Special Topics, 2013. **222**(7): p. 1553-1562.

21. Harne, R.L. and K.W. Wang, *A review of the recent research on vibration energy harvesting via bistable systems.* Smart Materials and Structures, 2013. **22**(2): p. 023001.

22. Arrieta, A., S. Neild, and D. Wagg, *Nonlinear dynamic response and modeling of a bi-stable composite plate for applications to adaptive structures.* Nonlinear Dynamics, 2009. **58**(1): p. 259-272.

23. Arrieta, A.F., S.A. Neild, and D.J. Wagg, *On the cross-well dynamics of a bi-stable composite plate.* Journal of Sound and Vibration, 2011. **330**(14): p. 3424-3441.

24. Diaconu, C.G., P.M. Weaver, and A.F. Arrieta, *Dynamic analysis of bi-stable composite plates.* Journal of Sound and Vibration, 2009. **322**(4): p. 987-1004.

25. Vogl, G.A. and M.W. Hyer, *Natural vibration of unsymmetric cross-ply laminates.* Journal of Sound and Vibration, 2011. **330**(20): p. 4764-4779.

26. Arrieta, A.F., et al., *Low order model for the dynamics of bi-stable composite plates.* Journal of Intelligent Material Systems and Structures, 2011. **22**(17): p.

2025-2043.

27. Taki, M.S., et al., *Dynamic responses of cross-ply bi-stable composite laminates with piezoelectric layers.* Archive of Applied Mechanics, 2016. **86**(6): p. 1003-1018.

28. Peeters, L., P. Powell, and L. Warnet, *Thermally-induced shapes of unsymmetric laminates.* Journal of Composite Materials, 1996. **30**(5): p. 603-626.

29. M.W.Hyer, *Calculations of the Room-Temperature Shapes of Unsymmetric Laminates.* Composite Materials, 1981. **15**: p. 296-310.

30. Aimmanee, S. and M. Hyer, *Analysis of the manufactured shape of rectangular THUNDER-type actuators.* Smart materials and structures, 2004. **13**: p. 1389.

31. Pirrera, A., D. Avitabile, and P. Weaver, *Bistable plates for morphing structures: A refined analytical approach with high-order polynomials.* International journal of solids and structures, 2010. **47**(25-26): p. 3412-3425.

32. Ashton, J.E., *Approximate Solutions for Unsymmetrically Laminated Plates.* Journal of Composite Materials, 1969. **3**: p. 189-191.

33. Gigliotti, M., et al., *Predicting loss of bifurcation behaviour of 0/90 unsymmetric composite plates subjected to environmental loads.* Composite Structures, 2012.

34. Arrieta, A., D. Wagg, and S. Neild, *Dynamic snap-through for morphing of bi-stable composite plates.* Journal of Intelligent Material Systems and Structures, 2011. **22**: p. 103-112.